Table 3 Logistic regression analysis of the occurrence of major complications in the propensity score-matched groups

	OR	95% CI	p
Treatment			
Control	Reference		
High-dose methylprednisolone	1.66	1.23 to 2.24	0.001
Sex			
Male	Reference		
Female	0.57	0.38 to 0.86	0.007
Age			
≤59	Reference		
60–69	1.49	1.04 to 2.12	0.029
70–79	1.81	1.26 to 2.62	0.002
≥80	2.07	1.27 to 3.39	0.004
Charlson Comorbidity Index			
1	Reference		
2	1.41	1.04 to 1.92	0.027
≥3	1.95	1.26 to 3.02	0.003
Japan Coma Scale at admission			
0 (alert)	Reference		
1–3 (drowsy)	1.51	0.99 to 2.31	0.059
10–30 (somnolence)	1.75	0.74 to 4.09	0.200
100–300 (coma)	4.55	2.06 to 10.06	<0.001
Cervical spinal surgery	1.95	1.44 to 2.64	<0.001
Hospital volume (per year)	1.01	0.99 to 1.03	0.550

DPC database, which covers approximately 40% of all acute hospitalisations in Japan, enabled us to conduct a nationwide investigation. In addition, the propensity score-matched analysis allowed us to evaluate the risks of high-dose methylprednisolone treatment while controlling for confounding variables, an assessment that prior studies have been unable to make.

Certain characteristics of the study subjects warrant mention. First, the mean age of the patients in this study was substantially higher than in other SCI studies, which may be explained by the rapid aging of our society. Currently, the geriatric population (those 65 years of age or older) accounts for approximately 23% of the Japanese population. Second, the surgery rate reported in this study was markedly lower compared with that of North American or European countries. The low surgery rate likely reflects differences in patient demographics and treatment strategy. In Japan, approximately 70% of patients sustain a cervical SCI without bone injury, such as fracture or dislocation (mostly elderly patients), and conservative treatment is recommended for these patients.

Our study has several limitations. First, as is common in studies using administrative data, coded diagnoses and outcomes are less well validated than prospective surveys. A degree of misclassification or under-reporting of outcome might have occurred in this study. Second, the DPC database does not provide important clinical data, such as severity of paralysis (ie, Frankel classification) at admission, patient disability at discharge, and cause of death. We could not confirm whether the administration of methylprednisolone conformed to the NASCIS protocol. Specifically, administrative databases such as the DPC database and National Inpatient Sample provide only limited information on the baseline neurological status, which is one of the most important factors that affect morbidity after SCI. It is possible that the high-dose methylprednisolone group included patients with more severe impairment than the control group, which would have created a bias toward overestimating the adverse effect of the high-dose methylprednisolone. Finally, although propensity-score adjustment is currently recognised as the best analytical approach for retrospective observational data, unmeasured confounders might have caused a hidden selection bias.

Comparison with other studies

Most published studies following the NASCIS trials indicated an increased overall complication rate after high-dose methylprednisolone treatment.[11–15] Regarding specific complications, pneumonia,[11–13 15] infection,[11 12] and gastrointestinal bleeding[13] are the most common complications reported in the literature, in patients receiving high-dose methylprednisolone. However, available evidence on the adverse effects of high-dose methylprednisolone is mixed, with substantial variation in reported incidences, and even conflicting results. There are several studies reporting lower complication rates in high-dose methylprednisolone groups.[22 23] Major drawbacks of these previous studies were small sample size and lack of adjustment for confounding variables, which considerably limits the validity of their conclusion.

In the present study, we first analysed the possible adverse impact of high-dose methylprednisolone treatment in SCI patients using a large nationwide database. We then performed propensity score-matched analysis to adjust for potential confounding factors. High-dose methylprednisolone was associated with a significantly higher risk of complications (17.7% vs 11.8%, p=0.001) than control after adjustment for confounding variables. Specifically, we found a significant increase in the occurrence of gastrointestinal ulcer/bleeding (8.4% vs 3.8%, p<0.001) in the high-dose methylprednisolone group.

In this study, we observed slightly lower in-hospital mortality in patients receiving high-dose methylprednisolone (2.8% in the methylprednisolone group vs 3.0% in the control group after propensity-score matching). The impact of high-dose methylprednisolone on patient survival remains unclear. The CRASH trial,[24] a randomised trial which examined the efficacy of high-dose methylprednisolone in the treatment of head injury patients, was prematurely terminated because of increased 2-week mortality in the high-dose methylprednisolone group (21.1% vs 17.9%). However, it remains to be determined whether these findings are generalisable to patients sustaining acute SCI. In fact, reported mortalities in SCI patients in the literature have been slightly more favourable in those with high-dose methylprednisolone treatment,[12 15 23] although sample bias played a substantial role. Similarly, a meta-analysis[18] of 51 randomised trials of high-dose methylprednisolone in elective and trauma surgery found reduced mortality compared with controls (1.7% vs 2.7%), although it was not statistically significant. In our propensity score-matched analysis, no significant difference in mortality was observed between the groups in spite of a significant increase in complication rate in patients receiving high-dose methylprednisolone, which may be partly attributable to advances in intensive care and increased physician awareness of steroid-related complications.

Implications for future research

We believe that the findings of our study will provide a basis for future research to re-examine the net benefit of high-dose methylprednisolone treatment described in the NASCIS trials. The main criticism of the NASCIS trials is two-fold: (1) there was no significant difference in the primary comparison; a significant but small benefit (ie, five points in motor score) was found only after posthoc subgroup analysis; (2) there was a trend toward an increase in adverse events, including

pneumonia, infection and gastrointestinal bleeding in patients receiving high-dose methylprednisolone. For the reasons stated above, current guidelines classify this treatment only as a therapeutic 'option', leaving the decision to adopt or avoid this treatment up to individual physicians. Despite the apparent need for a randomised study of better design with sufficient power to examine whether the beneficial effect of high-dose methylprednisolone is reproducible, no such study has been conducted mainly because of ethical and safety concerns. With a dearth of effective alternative therapeutic options, we believe that a strong case exists for a randomised placebo-controlled trial re-examining the potential benefit of high-dose methylprednisolone in patients sustaining SCI. The results of our study showed that high-dose methylprednisolone treatment was not associated with any increase in in-hospital mortality, despite a significant increase in complications, a finding that further justifies future randomised trials in carefully selected patient population. To minimise the heterogeneity of the study population, future trials should focus on patients with incomplete SCI, in whom a beneficial effect was observed in the NASCIS trial. According to an estimate by the International Campaign for Cures of Spinal Cord Injury Paralysis,[25] it would require about 450 subjects with incomplete motor cervical SCI in each arm of the study to show a statistically significant difference of five American Spinal Injury Association motor points between the experimental and control groups. It would clearly require a multi-institution collaboration to carry out this project.

CONCLUSION

Despite controversies lingering for more than two decades since the publication of the NASCIS trial, risks and benefits of high-dose methylprednisolone treatment remain unclear with limited high-level evidence. In this study, we focused on safety concerns of high-dose methylprednisolone treatment, and first clarified the magnitude of its adverse impact by using a large nationwide database. There was a significantly increased risk of major complications, in particular, gastrointestinal ulcer/bleeding, with high-dose methylprednisolone, but no increase in in-hospital mortality. We believe that the findings of our study provides critical information on the risks associated with high-dose methylprednisolone administration in patients with SCI, and thus, may help physicians make a more informed decision on the use of this highly controversial treatment.

Contributors HC, HY, KT, HK and ST contributed to the conception and design of the study. HH, KO, KF contributed to the analysis, and all authors contributed to the interpretation. HC drafted the article; all authors revised it critically for important intellectual content and approved the final version submitted for publication. HC is the guarantor. All authors had full access to all of the data in the study and can take responsibility for the integrity of the data and the accuracy of the data analysis.

Funding This study was funded by a Grant-in-Aid for Research on Policy Planning and Evaluation from the Ministry of Health, Labour and Welfare, Japan (Grant number: H22-Policy-031), by a Grant-in-Aid for Research on Intractable Diseases from the Ministry of Health, Labour and Welfare, Japan (Grant number: H23-Nanchi-032), by a Grant-in-Aid for Scientific Research B (No. 22390131) from the Ministry of Education, Culture, Sports, Science and Technology, and by the Funding Program for World-Leading Innovative R&D on Science and Technology (FIRST programme) from the Council for Science and Technology Policy, Japan (Grant number: 0301002001001). The researchers were independent from the funders. Sponsors played no role in the study design; the collection, analysis, and interpretation of data; the writing of the article; or the decision to submit it for publication.

Competing interests All authors have completed the Unified Competing Interest form at http://www.icmje.org/coi_disclosure.pdf (available on request from the corresponding author) and declare that (1) none has company support for the submitted work; (2) the authors have no relationships with companies that might have an interest in the submitted work in the previous 3 years; (3) their spouse, partners, or children have no financial relationships that may be relevant to the submitted work; and (4) the authors have no non-financial interests that may be relevant to the submitted work.

Ethics approval The Institutional Review Board at The University of Tokyo approved the study.

Provenance and peer review Not commissioned; externally peer reviewed.

REFERENCES

1 Bracken MB, Shepard MJ, Collins WF, *et al*. A randomized, controlled trial of methylprednisolone or naloxone in the treatment of acute spinal-cord injury. Results of the Second National Acute Spinal Cord Injury Study. *N Eng J Med* 1990;322:1405–11.
2 Bracken MB, Shepard MJ, Holford TR, *et al*. Administration of methylprednisolone for 24 or 48 hours or tirilazad mesylate for 48 hours in the treatment of acute spinal cord injury. Results of the Third National Acute Spinal Cord Injury Randomized Controlled Trial. National Acute Spinal Cord Injury Study. *JAMA* 1997;277:1597–604.
3 Sayer FT, Kronvall E, Nilsson OG. Methylprednisolone treatment in acute spinal cord injury: the myth challenged through a structured analysis of published literature. *Spine J* 2006;6:335–43.
4 Hurlbert RJ. The role of steroids in acute spinal cord injury: an evidence-based analysis. *Spine (Phila Pa 1976)* 2001:S39–46.
5 Short DJ, El Masry WS, Jones PW. High dose methylprednisolone in the management of acute spinal cord injury—a systematic review from a clinical perspective. *Spinal Cord* 2000;38:273–86.
6 Eck JC, Nachtigall D, Humphreys SC, *et al*. Questionnaire survey of spine surgeons on the use of methylprednisolone for acute spinal cord injury. *Spine (Phila Pa 1976)* 2006;31:E250–3.
7 Frampton AE, Eynon CA. High dose methylprednisolone in the immediate management of acute, blunt spinal cord injury: what is the current practice in emergency departments, spinal units, and neurosurgical units in the UK? *Emerg Med J* 2006;23:550–3.
8 Molloy S, Price M, Casey AT. Questionnaire survey of the views of the delegates at the European Cervical Spine Research Society meeting on the administration of methylprednisolone for acute traumatic spinal cord injury. *Spine (Phila Pa 1976)* 2001;26:E562–4.
9 Rozet I. Methylprednisolone in acute spinal cord injury: is there any other ethical choice? *J Neurosurg Anesthesiol* 2008;20:137–9.
10 Bracken MB. Steroids for acute spinal cord injury. *Cochrane Database Syst Rev* 2012;1:CD001046.
11 Ito Y, Sugimoto Y, Tomioka M, *et al*. Does high dose methylprednisolone sodium succinate really improve neurological status in patient with acute cervical cord injury?: a prospective study about neurological recovery and early complications. *Spine (Phila Pa 1976)* 2009;34:2121–4.
12 Suberviola B, González-Castro A, Llorca J, *et al*. Early complications of high-dose methylprednisolone in acute spinal cord injury patients. *Injury* 2008;39:748–52.
13 Matsumoto T, Tamaki T, Kawakami M, *et al*. Early complications of high-dose methylprednisolone sodium succinate treatment in the follow-up of acute cervical spinal cord injury. *Spine (Phila Pa 1976)* 2001;26:426–30.
14 Pointillart V, Petitjean ME, Wiart L, *et al*. Pharmacological therapy of spinal cord injury during the acute phase. *Spinal Cord* 2000;38:71–6.
15 Gerndt SJ, Rodriguez JL, Pawlik JW, *et al*. Consequences of high-dose steroid therapy for acute spinal cord injury. *J Trauma* 1997;42:279–84.
16 Matsuda S, Ishikawa K, Kuwabara K, *et al*. Development and use of the Japanese case-mix system. *Eurohealth* 2008;14:27–30.
17 Chikuda H, Yasunaga H, Horiguchi H, *et al*. Mortality and morbidity in dialysis-dependent patients undergoing spinal surgery: analysis of a national administrative database in Japan. *J Bone Joint Surg Am* 2012;94:433–8.
18 Sauerland S, Nagelschmidt M, Mallmann P, *et al*. Risks and benefits of preoperative high dose methylprednisolone in surgical patients: a systematic review. *Drug Saf* 2000;23:449–61.
19 Ono K, Wada K, Takahara T, *et al*. Indications for computed tomography in patients with mild head injury. *Neurol Med-Chir* 2007;47:291–7.
20 Quan H, Sundararajan V, Halfon P, *et al*. Coding algorithms for defining comorbidities in ICD-9-CM and ICD-10 administrative data. *Med Care* 2005;43:1130–9.
21 Ayanian JZ, Landrum MB, Guadagnoli E, *et al*. Specialty of ambulatory care physicians and mortality among elderly patients after myocardial infarction. *N Engl J Med* 2002;347:1678–86.

22 Tsutsumi S, Ueta T, Shiba K, *et al*. Effects of the Second National Acute Spinal Cord Injury Study of high-dose methylprednisolone therapy on acute cervical spinal cord injury-results in spinal injuries center. *Spine (Phila Pa 1976)* 2006;31:2992–6.
23 George ER, Scholten DJ, Buechler CM, *et al*. Failure of methylprednisolone to improve the outcome of spinal cord injuries. *Am Surg* 1995;61: 659–63.
24 Roberts I, Yates D, Sandercock P, *et al*. Effect of intravenous corticosteroids on death within 14 days in 10008 adults with clinically significant head injury (MRC CRASH trial): randomised placebo-controlled trial. *Lancet* 2004;364:1321–8.
25 Fawcett JW, Curt A, Steeves JD, *et al*. Guidelines for the conduct of clinical trials for spinal cord injury as developed by the ICCP panel: spontaneous recovery after spinal cord injury and statistical power needed for therapeutic clinical trials. *Spinal Cord* 2007;45:190–205.

Appendix Japan Coma Scale for grading of impaired consciousness[19]

Grade	Consciousness level
1-digit code	The patient is awake without any stimuli, and is:
1	Almost fully conscious
2	Unable to recognise time, place and person
3	Unable to recall name or date of birth
2-digit code	The patient can be aroused (then reverts to previous state after cessation of stimulation):
10	Easily by being spoken to (or is responsive with purposeful movements, phrases, or words)*
20	With loud voice or shaking of shoulders (or is almost always responsive to very simple words like yes or no, or to movements)*
30	Only by repeated mechanical stimuli
3-digit code	The patient cannot be aroused with any forceful mechanical stimuli, and:
100	Responds with movements to avoid the stimulus
200	Responds with slight movements including decerebrate and decorticate posture
300	Does not respond at all except for change of respiratory rhythm

'R' and 'I' are added to the grade to indicate restlessness and incontinence of urine and faeces, respectively: for example; 100-R and 30-RI.
*Criteria in parentheses are used in patients who cannot open their eyes for any reason.

The Journal of Arthroplasty 28 (2013) 766–771

Contents lists available at SciVerse ScienceDirect

The Journal of Arthroplasty

journal homepage: www.arthroplastyjournal.org

An Additional Reference Axis Improves Femoral Rotation Alignment in Image-Free Computer Navigation Assisted Total Knee Arthroplasty

Hiroshi Inui MD, Shuji Taketomi MD, Kensuke Nakamura MD, Takaki Sanada MD, Sakae Tanaka MD, Takumi Nakagawa MD

Department of Orthopaedic Surgery, Faculty of Medicine, The University of Tokyo, Tokyo, Japan

ARTICLE INFO

Article history:
Received 17 August 2012
Accepted 28 January 2013

Keywords:
total knee arthroplasty
image-free navigation
femoral rotation
surgical transepicondylar axis
condylar twist angle

ABSTRACT

Few studies have demonstrated improvement in accuracy of rotational alignment using image-free navigation systems mainly due to the inconsistent registration of anatomical landmarks. We have used an image-free navigation for total knee arthroplasty, which adopts the average algorithm between two reference axes (transepicondylar axis and axis perpendicular to the Whiteside axis) for femoral component rotation control. We hypothesized that addition of another axis (condylar twisting axis measured on a preoperative radiograph) would improve the accuracy. One group using the average algorithm (double-axis group) was compared with the other group using another axis to confirm the accuracy of the average algorithm (triple-axis group). Femoral components were more accurately implanted for rotational alignment in the triple-axis group (ideal: triple-axis group 100%, double-axis group 82%, $P<0.05$).

Total knee arthroplasty (TKA) has become one of the most successful surgical procedures in orthopedic surgery [1,2]. The success of this procedure depends on many factors, including surgical techniques and the design and material of the components. With regard to surgical techniques, implant positioning and soft tissue balancing are very important. Malpositioning of any component can lead to an increased risk of loosening, instability, patella subluxation, and residual pain [3–5].

Computer-assisted navigation systems have been designed to increase the accuracy of implantation and have become much more accepted and prevalent in recent years. Several studies have demonstrated superior alignment of components in the coronal plane in navigated TKA compared with conventionally implanted TKA [6–8]. However, with regard to the accuracy of rotational alignment, few studies have demonstrated an improvement in computer-assisted navigation as compared with conventional methods. In particular, using image-free navigation systems, many authors have reported variability in identifying the surgical transepicondylar axis (SEA) for femoral rotation [9–11]. The Whiteside axis is generally assumed to be perpendicular to SEA and therefore a reliable axis of reference [12,13]. However, criticism of this landmark also includes difficulty in identification in case of trochlear dysplasia or destructive arthritis [14,15]. Using an average algorithm between the determined angle of the registered Whiteside axis and transepicondylar axis has been recommended, and Stockl et al. showed that image-free navigation using this algorithm improved femoral rotational alignment [15,16]. However, much room for improvement in femoral component rotation control remains in the use of image-free navigation systems.

To reduce the registration errors, we believed that there is a need for an additional reference axis to confirm the accuracy of the rotational axis calculated by the image-free navigation system using an average algorithm. If the additional axis contradicts the rotational axis calculated by the image-free navigation system, it shows the necessity to re-register such landmarks as the medial sulcus, lateral epicondyle, and femoral AP axis. The posterior condylar axis (PCA) is known to be one of the most common axes during conventional total knee arthroplasty procedure. However, there are differences among patients in the angle between SEA and PCA, which is often called the condylar twist angle (CTA); therefore, CTA must be measured preoperatively to accurately set the rotational cutting guide in the conventional technique. Indeed, the use of computed tomography (CT) or magnetic resonance imaging (MRI) is recommended to detect CTA, but this accompanies some disadvantages, including the additional cost of CT and MRI and the additional radiation dose associated with CT. However, there have been some reports on methods that can help us to predict PCA and CTA preoperatively from radiography alone [17–19]. Just one additional radiograph is less of a disadvantage than CT or MRI.

The purpose of this study was to clarify whether the accuracy of the femoral rotational axis derived from an image-free navigation

The Conflict of Interest statement associated with this article can be found at http://dx.doi.org/10.1016/j.arth.2013.01.030.

Reprint requests: Hiroshi Inui, MD, Department of Orthopaedic Surgery, Faculty of Medicine, The University of Tokyo, 7-3-1 Hongo, Bunkyo-ku, Tokyo 113-0033, Japan.

0883-5403/2805-0011$36.00/0 – see front matter © 2013 Elsevier Inc. All rights reserved.
http://dx.doi.org/10.1016/j.arth.2013.01.030

system using an average algorithm could be confirmed by calculating another reference axis determined by PCA and CTA predicted from one additional radiograph, and also whether this improved femoral rotational alignment. We therefore hypothesized that this confirmation using the additional axis would improve femoral rotational alignment.

Materials and Methods

Institutional review board approval was received for this study. All patients provided written informed consent.

Of a total of 162 consecutive primary TKA procedures performed in 146 patients between January 2009 and September 2011, 158 knees were replaced using the Stryker 4.0 image-free computer navigation system (Stryker Orthopedics, Mahwah, NJ) equipped with an average algorithm derived from the registered the Whiteside axis and SEA.

Between January 2009 and June 2010, femoral rotational alignment was determined according to this navigation algorithm (double-axis group: 78 knees) and between July 2010 and September 2011, femoral rotational alignment was determined by the navigation system and confirmed by the additional axis (triple-axis group: 80 knees). With power set at 0.80 and a 2-sided P-value of 0.05, we calculated 24 patients would be needed in each group to detect the accuracy of the femoral rotational alignment. Thirty-eight knees in the double-axis group and 26 knees in the triple-axis group were assessed by axial CT imaging after surgery. Preoperative variables were recorded, including age, sex, body mass index, preoperative diagnosis, frontal alignment, and range of motion. Pre-operative scores were obtained using the Knee Society Score (KSS) [20]. There was no statistically significant difference between the groups in terms of demographic characteristics (Table 1).

Pre-Operative Planning

Preoperatively, in the triple-axis group, one radiograph of the distal femur was taken by the method of Kanekasu et al. [17], and we contrived to see the epicondyles and posterior condyles of the femur by radiography as accurately as by axial CT imaging. We measured the angle between the clinical epicondylar axis (CEA) and PCA on the radiograph (Fig. 1). Then, we considered the influences of two things. One was the angle between CEA and SEA which had been reported to be 3° [18]. The other was the residual articular cartilage of the posterior condyle which the radiograph was unable to detect (Fig. 2). Takashiro et al. [19] demonstrated that the articular cartilage wear of the posterior femoral condyle affected CTA and that the articular cartilage wear of the posterior femoral condyle of patients with varus knees was mainly localized in the posteromedial condyle. We assumed that the cartilage wear would localized in the posterolatelal condyle of patients with valgus knees and the cartilage wear of the posteromedial and posterolateral condyle of patients with neutral knees would be equal, and that the angle affected by the cartilage wear was 1° [19]. Therefore, we subtracted 4° (=3°+1°) from the measured angle for varus knees, 3° for neutral knees, and 2° (=3°–1°) for valgus knees in this study to attain the predicted condylar twist angle (p-CTA) (Fig. 2). The average p-CTA was 3.7°±1.0° of external rotation [mean±standard deviation (SD), range: 1°–7° of external rotation].

Table 1
Preoperative Demographic Data.

	Double-Axis Group	Triple-Axis Group	*P*-Value
Number of patients	38	26	
Sex (female/male)	32/6	21/5	
Diagnosis (OA/AN)	36/2	24/2	
Age (years)	76.8±4.6	79.6±5.1	n.s.
Pre-operative FTA (°)	185.6±9.6	186.5±6.0	n.s.
Pre-operative KSS	36.4±10.1	34.9±9.7	n.s.
Maximum extension (°)	−10.9±6.7	−9.4±6.1	n.s.
Maximum flexion (°)	120.3±14.2	120.0±11.8	n.s.
Body mass index (kg/m^2)	25.6±3.9	25.2±3.5	n.s.

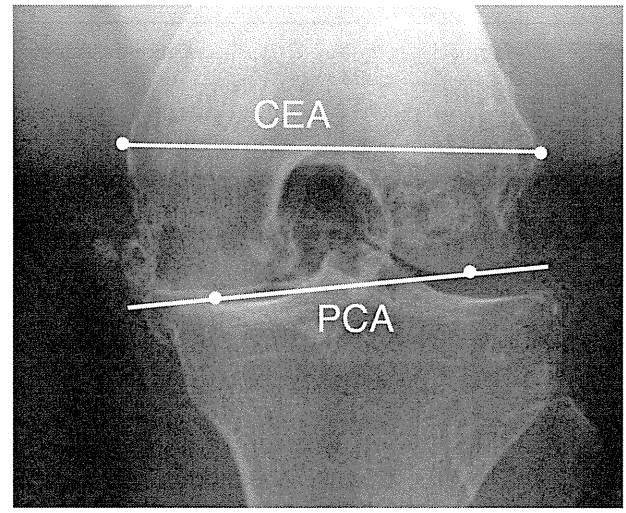

Fig. 1. Axial radiograph of the distal femur taken by the method of Kanekasu et al. [17]. CEA is the line connecting the medial and lateral epicondylar prominences; PCA is the line connecting the posterior margins of the medial and lateral femoral condyles.

Surgical Procedure

The Stryker 4.0 Navigation System was used for computer-assisted implantation. The system was image-free and used infrared cameras and light-emitting diodes. Surgery was performed under a tourniquet. A midvastus approach was used for varus and neutral knees and a medial parapatellar approach was used for valgus knees. The patella was everted in all patients. Landmarks comprised the center of the femoral head, the distal femur, the proximal tibia, the ankle, the Whiteside axis, the epicondylar axis (lateral epicondyle, medial sulcus), the anterior surface of the distal femoral cortex, the condylar surfaces of the femur and tibia, and the tibial AP axis. The femoral rotation axis on the navigation system (navi-FRA) was defined as the average rotational axis of the transepicondylar axis and the axis perpendicular to the Whiteside axis in the double-axis group (Fig. 3).

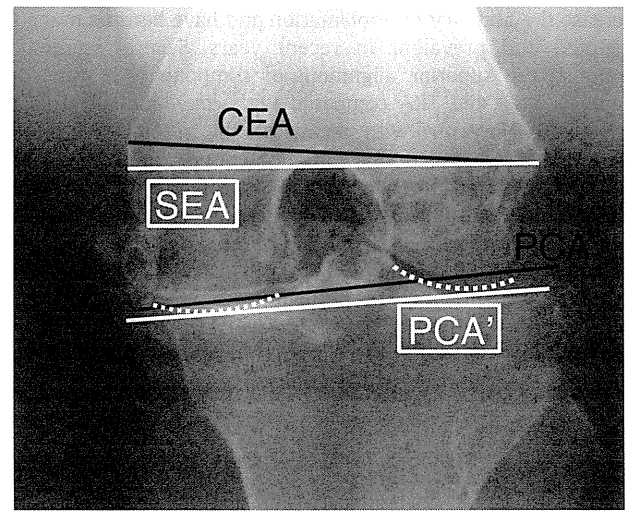

Fig. 2. Predicted condylar twist angle (p-CTA). P-CTA is the angle between SEA and PCA'. PCA' is the line connecting the posterior margins of the two dotted curves which are the assumed posterior femoral condyles with the articular cartilage included.

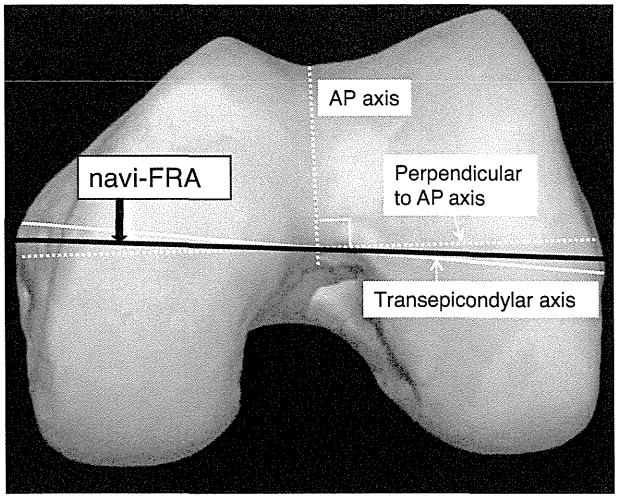

Fig. 3. The femoral rotation axis on the navigation system ("navi-FRA"). Navi-FRA is defined as the average axis of the transepicondylar axis and the axis perpendicular to the AP axis. AP axis = Whiteside's line.

In the triple-axis group, after cutting the distal femur, the posterior reference guide was set. Using the posterior reference guide, we drew two blue lines, one of which was "p-CTA −2°" externally rotated from PCA and the other was the "p-CTA +2°" externally rotated (Fig. 4). We measured the angles between navi-FRA and the two lines intraoperatively using the navigation template drilling guide. The guide was one of the specific adapted instruments of the Stryker 4.0 system which was developed to calculate the angle between PCA and the line connecting two drill holes or between PCA and the lower end of the guide (Fig 5). If the former angle was displayed as "internal" and the latter as "external," we concluded that navi-FRA was set as accurately as possible since the differences between navi-FRA and the axis determined by PCA and p-CTA were within 2° (Fig. 5). If both angles were displayed as internal or external, we assumed that the registration had not been performed accurately, and we re-registered the three landmarks (lateral epicondyle, medial sulcus, and the Whiteside axis). After one more registration, we followed navi-FRA and set the 4-in-1 cutting block.

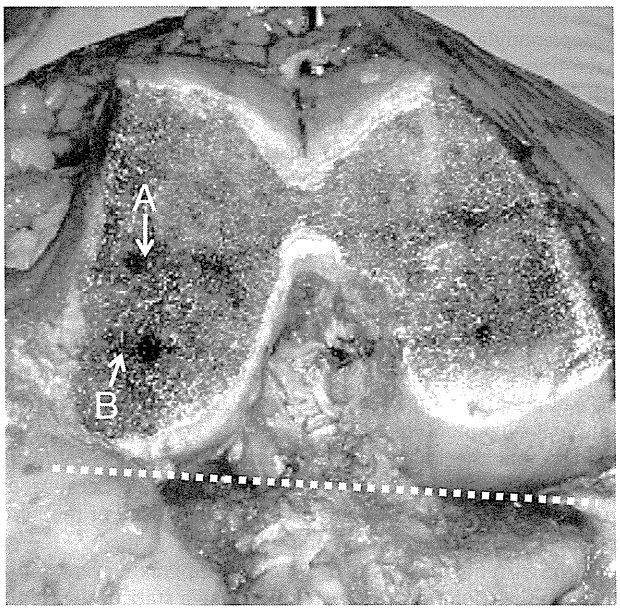

Fig. 4. Axial cross-section of the right distal femur. A: a blue line "p-CTA +2°" externally rotated from PCA. B: a blue line "p-CTA −2°" externally rotated from the PCA. PCA is the dotted line in this figure.

One surgeon (TN) took part in all procedures as the chief surgeon or first assistant. All implants used in both groups were Stryker Scopio NRG total knee implants.

Postoperative Evaluation

Rotational alignment of the femoral component was evaluated by CT. Knees were positioned in full extension. The rotational femoral component (RFC) angle was defined as the angle between the line through the center of both fixation pegs and SEA (Fig. 6). The ideal rotational femoral component angle was defined as falling within 3° of the target angle (0°) [9]. All CT scans were measured twice at 3-month intervals by two observers (HI and TS). Postoperative scores (KSS) and range of motion were recorded 1 year after operation.

Statistical Analysis

Data were analyzed using the EXCEL statistics 2008(SSRI Co., LTD., Tokyo, Japan) software package for Microsoft Windows. The Mann–Whitney U-test was used to compare the two groups. Fisher's exact probability test was used to compare the rate of optimally implanted components between the two groups. All significance tests were two-tailed, and a significance level of $P<0.05$ was used for all tests. The chance-corrected κ-coefficient was calculated to determine the intra- and inter-observer agreements. Kappa values of intra-observer reliability, inter-observer reliability (HI), and inter-observer reliability (TS) were 0.84, 0.91, and 0.92, respectively.

Results

The average RFC angle was $-0.1° \pm 2.4°$ [mean ± SD, range: 7° of internal rotation to 4° of external rotation] for the double-axis group and $0.3° \pm 1.7°$ (3° of external rotation to 3° of internal rotation) for the triple-axis group. With regard to the average RFC angle, there were no statistically significant differences observed between the two groups.

Thirty-one cases (82%) were implanted ideally (within 3° of neutral) in the double-axis group, whereas all 26 cases (100%) were implanted ideally in the triple-axis group. There was a statistically significant improvement in the triple-axis group ($P<0.05$) (Fig. 7).

In the triple-axis group, a second registration was necessary for 8 cases (31%). After re-registration, navi-FRA was set accurately in all cases. There were 2 cases in which both of the angles between navi-FRA and the two blue lines after the second registration were displayed as internal and one case in which they were external.

The mean post-operative KSS was 91.7 (range: 79 to 100) for the double-axis group and 93.5 (75 to 100) for triple-axis group. The mean post-operative functional score was 72.2 (5 to 100) for the double-axis group and 74.7 (30 to 100) for triple-axis group. With regard to range of motion, the average maximum extension angle and flexion angle were −2.1° (−20° to 5°) and 115.8° (90° to 135°) for the double axis group, while −1.8° (−10° to 5°) and 118.2° (95° to 135°) for the triple-axis group. No significant difference was detected in these values for the two groups. There was one case of patella subluxation in the double-axis group which needed an additional operation of arthroscopic lateral release, the femoral component of which was 6° internally implanted.

Discussion

Malpositioning of any component can lead to an increased risk of loosening, instability, and pain [3,4]. Restoration of the tibiofemoral angle to within 3° of neutral during TKA is thought to be associated with a better outcome [4–6,21,22]. Computer-assisted navigation systems are designed to increase the accuracy of implantation, and have become much more accepted and prevalent in recent years.

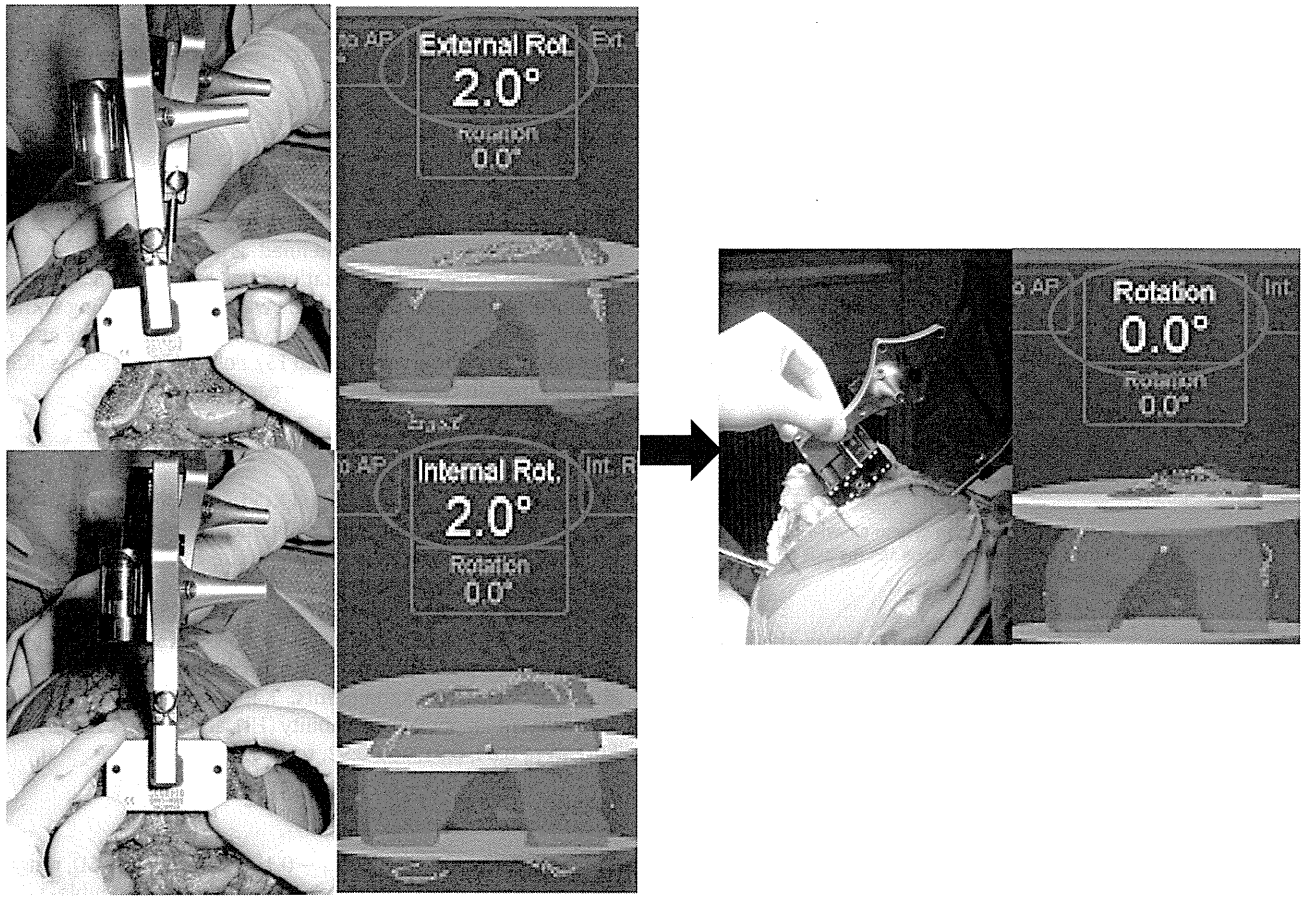

Fig. 5. Measurement of the angles between navi-FRA and the two lines (shown in Fig. 3) using the navigation system. If the two angles were displayed as "internal" and "external," we assumed navi-FRA to be accurate and set the 4-in-one cutting block in the neutral position.

Several studies have demonstrated superior alignment of the components in the coronal plane in navigated TKA compared with conventional implanted TKA [5,21,22].

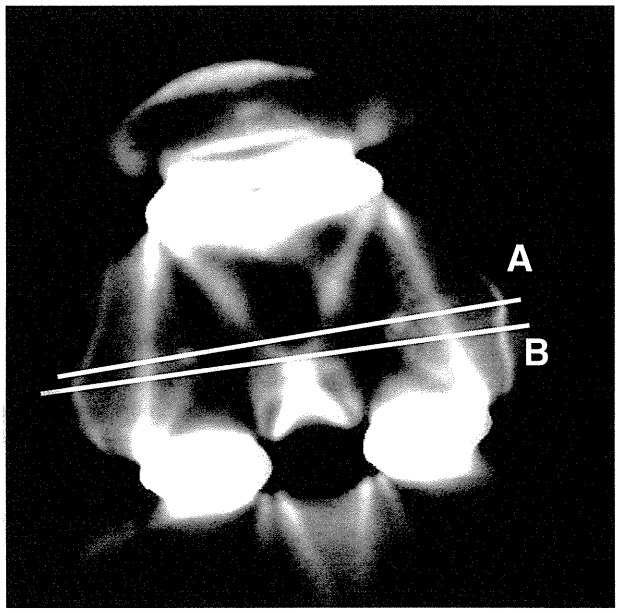

Fig. 6. Evaluation of rotational alignment of components on CT images. The rotational femoral component angle is defined as the angle between lines A and B. (A: Line through the center of both fixation pegs. B: Surgical epicondylar line).

Accurate rotational alignment of the femoral component is also considered important [5,9,10,18]. However, few studies have demonstrated an improvement in the accuracy of femoral rotational alignment with computer-assisted navigation, in particular image-free navigation, compared with conventional methods [9,10,16]. Many authors have reported variability in the identification of the transepicondylar axis [11,23]. Yau et al. [11] found that using the image-free navigation system, the maximum combined error was 8.2° with 5.3° at the medial and 2.9° at the lateral femoral epicondyles in the transepicondylar axis. Some authors have speculated that this variability is caused by soft tissue coverage [13,24]. However, in a cadaveric study, Siston et al. [25] demonstrated high variability even after all soft tissues had been stripped.

In our current series, eighty-two percent of femoral components in the double-axis group (31 of 37 knees) were implanted ideally. This result appears superior to those reported in previous studies using conventional techniques and that may be partly because of the average algorithm equipped with the Stryker 4.0 image-free navigation system [9,16,26]. However, Mizu-uchi et al. [9] demonstrated that 89.3% of femoral components were implanted within 3° of the ideal rotational alignment in the CT-based navigation group, and they reported that the image-free navigation systems are more widely used than the CT-based navigation systems not because of the accuracy of the former but because of the necessity of the latter for pre-operative CT scans and planning time.

In the current study, 100% of femoral components were implanted ideally in the triple-axis group, representing a statistically significant improvement ($P<0.05$). This result demonstrates that each reference axis (transepicondylar axis, Whiteside's axis, and posterior condylar axis) has some variability and is not always reliable; however,

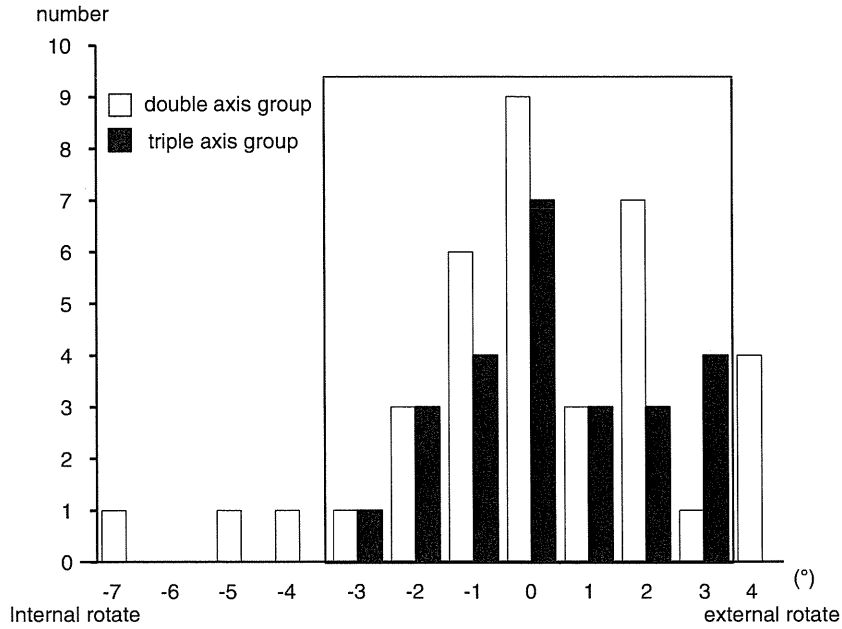

Fig. 7. Distribution of the rotational femoral component angle. The box represents the ideal alignment (±3° of neutral).

combination of a triple reference axis reduced variability, enabling the femoral component to be ideally implanted each time with respect to rotational alignment.

In the triple axis group, we could confirm the accuracy of the femoral rotational registration by another reference axis. Re-registration of the landmarks was performed if necessary. As a result, all femoral implants were implanted ideally with regard to rotational alignment. Based on this result, it is speculated that it is not the navigation system itself but the surgeons' registration error which is mainly responsible for the inaccuracy of the femoral rotational alignment.

There are some limitations to the current study. One limitation is that as we couldn't assess every patient's CT, there might be some potential selection bias. Follow-up CT was performed to those who consented in spite of the demerits of the additional cost and radiation dose associated with CT. Therefore, the patients evaluated by CT might be possessing a better outcome and more motivated than those who did not consent. The mean post-operative KSS, functional score, maximum extension angle and flexion angle of those who didn't consent were 90.9, 73.1, −1.5° and 115.1° (double-axis group, 40patients) and 92.2, 73.8, −1.8° and 116.8° (triple-axis group, 52 patients) respectively. No significant difference was detected between those who consented and those who didn't in both groups. Therefore, we think there might not be any potential selection bias in this study. However, we should have evaluated every patient's CT. Another limitation is that surgery in the two groups was performed at different times. Some studies have shown that there is a so-called learning curve in navigated surgery, especially in early cases. Twenty to thirty implantations are said to be necessary before surgeons become accustomed to the navigation system and the average operating time reaches a plateau [27,28]. At our institute, 63 implantations using the image-free navigation system (Stryker 3.1) had been performed by the end of December 2008; therefore, our result might not have been affected by the learning curve. Furthermore, 79% of femoral implants were ideally implanted with respect to rotation using the Stryker 3.1, which was equipped with the same average algorithm. There might have been no learning curve with regard to identification of the femoral transepicondylar axis and the Whiteside axis.

In conclusion, our study demonstrates that the accuracy of femoral rotational alignment with the image-free navigation system, which uses the average algorithm between the transepicondylar axis and the Whiteside axis, can be significantly improved by the addition of another reference axis determined by PCA and CTA, and this can be predicted not by CT or MRI but from just one radiograph.

References

1. Vessely MB, Whaley AL, Harmsen WS, et al. Long-term survivorship and failure modes of 1000 cemented condylar total knee arthroplasties. Clin Orthop Relat Res 2006;452:28.
2. Lutzner J, Gunther KP, Kirschner S. Functional outcome after computer-assisted versus conventional total knee arthroplasty: a randomized controlled study. Knee Surg Sports Traumatol Arthrosc 2010;18:1339.
3. Nicoll D, Rowley DI. Internal rotational error of the tibial component is a major cause of pain after total knee replacement. J Bone Joint Surg Br 2010;92:1238.
4. Jeffery RS, Morris RW, Denham RA. Coronal alignment after total knee replacement. J Bone Joint Surg Br 1991;73:709.
5. Abadie P, Galaud B, Michaut M, et al. Distal femur rotational alignment and patellar subluxation: a CT scan in vivo assessment. Orthop Traumatol Surg Res 2009;95:267.
6. Matziolis G, Krocker D, Weiss U, et al. A prospective, randomized study of computer-assisted and conventional total knee arthroplasty. Three-dimensional evaluation of implant alignment and rotation. J Bone Joint Surg Am 2007;89:236.
7. Longstaff LM, Sloan K, Stamp N, et al. Good alignment after total knee arthroplasty leads to faster rehabilitation and better function. J Arthroplasty 2009;24:570.
8. Mason JB, Fehring TK, Estok R, et al. Meta-analysis of alignment outcomes in computer-assisted total knee arthroplasty surgery. J Arthroplasty 2007;22:1097.
9. Mizu-uchi H, Matsuda S, Miura H, et al. The evaluation of post-operative alignment in total knee replacement using a CT-based navigation system. J Bone Joint Surg Br 2008;90:1025.
10. Chauhan SK, Clark GW, Lyoyd S, et al. Computer-assisted total knee replacement. A controlled cadaver study using a multi-parameter quantitative CT assessment of alignment (the Perth CT Protocol). J Bone Joint Surg Br 2004;86:818.
11. Yau WP, Leung A, Chiu KY, et al. Intraobserver errors in obtaining visually selected anatomic landmarks during registration process in nonimage-based navigation-assisted total knee arthroplasty: a cadaveric experiment. J Arthroplasty 2005;20:591.
12. Whiteside L, Arima J. The anteroposterior axis for femoral rotational alignment in valgus knee arthroplasty. Clin Orthop Relat Res 1995;321:168.
13. Arima J, Whiteside LA, McCarthy DS, et al. Femoral rotational alignment, based on the anteroposterior axis, in total knee arthroplasty in a valgus knee. J Bone Joint Surg Am 1995;77:1331.
14. Middleton FR, Palmer SH. How accurate is Whiteside's line as a reference axis in total knee arthroplasty? Knee 2007;14:204.
15. Vanin N, Panzica M, Dikos G, et al. Rotational alignment in total knee arthroplasty: intraoperative inter- and intraobserver reliability of Whiteside's line. Arch Orthop Trauma Surg 2011;131:1477.
16. Stockl B, Noquler M, Rosiek R, et al. Navigation improves accuracy of rotational alignment in total knee arthroplasty. Clin Orthop Relat Res 2004;426:180.
17. Kanekasu K, Makoto K, Kadoya Y. Axial radiography of the distal femur to assess rotational alignment in total knee arthroplasty. Clin Orthop Relat Res 2005;434:193.

18. Tashiro Y, Uemura M, Matsuda S, et al. Articular cartilage of the posterior condyle can affect rotational alignment in total knee arthroplasty. Knee Surg Sports Traumatol Arthrosc 2011 [Epub ahead of print].
19. Yoshino N, Takai S, Ohtsuka Y, et al. Computed tomography measurement of the surgical and clinical transepicondylar axis of the distal femur in osteoarthritic knees. J Arthroplasty 2001;16:493.
20. Insall JN, Dorr LD, Scott RD, et al. Rationale of the Knee Society clinical rating system. Clin Orthop Relat Res 1989;248:13.
21. Werner FW, Ayers DC, Maletsky LP, et al. The effect of valgus/varus malalignment on load distribution in total knee replacements. J Biomech 2005; 38:349.
22. Berger RA, Crossett LS, Jacobs JJ, et al. Malrotation causing patellofemoral complications after total knee arthroplasty. Clin Orthop Relat Res 1998;356:144.
23. Kinzel V, Ledger M, Shakespeare D. Can the epicondylar axis be defined accurately in total knee arthroplasty? Knee 2005;12:293.
24. Jenny JY, Boeri C. Low reproducibility of the intra-operative measurement of the transepicondylar axis during total knee replacement. Acta Orthop Scand 2004;75:74.
25. Siston RA, Patel JJ, Goodman SB, et al. The variability of femoral rotational alignment in total knee arthroplasty. J Bone Joint Surg Am 2005;87:2276.
26. Kim YH, Kim JS, Yoon SH. Alignment and orientation of the components in total knee replacement with and without navigation support: a prospective, randomised study. J Bone Joint Surg Br 2007;89:471.
27. Jenny JY, Miehlke RK, Giurea A. Learning curve in navigated total knee replacement. A multi-center study comparing experienced and beginner centers. Knee 2008;15:80.
28. Smith BR, Deakin AH, Baines J, et al. Computer navigated total knee arthroplasty: the learning curve. Comput Aided Surg 2010;15:40.

JOURNAL OF THE MECHANICAL BEHAVIOR OF BIOMEDICAL MATERIALS 31 (2014) 100–106

Available online at www.sciencedirect.com

ScienceDirect

www.elsevier.com/locate/jmbbm

Research Paper

Grafting of poly(2-methacryloyloxyethyl phosphorylcholine) on polyethylene liner in artificial hip joints reduces production of wear particles

Toru Moro[a,b,*], *Masayuki Kyomoto*[a,c,d], *Kazuhiko Ishihara*[c], *Kenichi Saiga*[a,c,d], *Masami Hashimoto*[e], *Sakae Tanaka*[b], *Hideya Ito*[b], *Takeyuki Tanaka*[b], *Hirofumi Oshima*[b], *Hiroshi Kawaguchi*[b], *Yoshio Takatori*[a,b]

[a]*Division of Science for Joint Reconstruction, Graduate School of Medicine, The University of Tokyo, 7-3-1 Hongo, Bunkyo-ku, Tokyo 113-8655, Japan*
[b]*Sensory & Motor System Medicine, Faculty of Medicine, The University of Tokyo, 7-3-1 Hongo, Bunkyo-ku, Tokyo 113-8655, Japan*
[c]*Department of Materials Engineering, School of Engineering, The University of Tokyo, 7-3-1 Hongo, Bunkyo-ku, Tokyo 113-8655, Japan*
[d]*Research Department, KYOCERA Medical Corporation, 3-3-31 Miyahara, Yodogawa-ku, Osaka 532-0003, Japan*
[e]*Materials Research and Development Laboratory, Japan Fine Ceramics Center, 2-4-1 Mutsuno, Atsuta-ku, Nagoya 456-8587, Japan*

ARTICLE INFO

Article history:
Received 20 April 2012
Received in revised form
7 March 2013
Accepted 18 March 2013
Available online 17 April 2013

Keywords:
Artificial hip joint
Total hip arthroplasty
Periprosthetic osteolysis
Aseptic loosening
Polyethylene
Surface modification

ABSTRACT

Despite improvements in the techniques, materials, and fixation of total hip arthroplasty, periprosthetic osteolysis, a complication that arises from this clinical procedure and causes aseptic loosening, is considered to be a major clinical problem associated with total hip arthroplasty. With the objective of reducing the production of wear particles and eliminating periprosthetic osteolysis, we prepared a novel hip polyethylene (PE) liner whose surface graft was made of a biocompatible phospholipid polymer—poly(2-methacryloyloxyethyl phosphorylcholine (MPC)). This study investigated the wear resistance of the poly(MPC)-grafted cross-linked PE (CLPE; MPC-CLPE) liner during 15×10^6 cycles of loading in a hip joint simulator. The gravimetric analysis showed that the wear of the acetabular liner was dramatically suppressed in the MPC-CLPE liner, as compared to that in the non-treated CLPE liner. Analyses of the MPC-CLPE liner surface revealed that it suffered from no or very little wear even after the simulator test, whereas the CLPE liners suffered from substantial wears. The scanning electron microscope (SEM) analysis of the wear particles isolated from the lubricants showed that poly(MPC) grafting dramatically decreased the total number, area, and volume of the wear particles. However, there was no significant difference in the particle size distributions, and, in particular, from the SEM image, it was observed that particles with diameters less than 0.50 μm were present in the range of the highest frequency. In addition, there were no significant differences in the particle size descriptors and particle shape descriptors.

*Corresponding author at: Division of Science for Joint Reconstruction, Graduate School of Medicine, The University of Tokyo, 7-3-1 Hongo, Bunkyo-ku, Tokyo 113-8655, Japan. Tel.: +81 3 3815 5411x30474; fax: +81 3 3818 4082.
E-mail address: moro-ort@h.u-tokyo.ac.jp (T. Moro).

1751-6161/$ - see front matter
http://dx.doi.org/10.1016/j.jmbbm.2013.03.011

The results obtained in this study show that poly(MPC) grafting markedly reduces the production of wear particles from CLPE liners, without affecting the size of the particles. These results suggest that poly(MPC) grafting is a promising technique for increasing the longevity of artificial hip joints.

1. Introduction

Sir John Charnley introduced the use of polyethylene (PE) components in total hip arthroplasty (THA) in the 1960s, and since then, these components have been extensively used for 50 years (Charnley, 1961). However, aseptic loosening resulting from periprosthetic osteolysis—which is a clinical complication arising from THA—is the prevalent cause of revision surgery (Bozic et al., 2009). Previous studies have revealed that PE particles generated from liners play a major etiological role in periprosthetic osteolysis. Macrophage phagocytosis of the PE particles is followed by the secretion of prostaglandin E2 (PGE2) and cytokines, which induce the receptor activator of the NF-κB ligand (RANKL) expression, consequently resulting in osteoclastogenesis and bone resorption (Harris, 2004; Jacobs et al., 2001). Further, periprosthetic osteolysis is closely related to the rate of PE wear and the characteristics of the wear particles (Catelas and Jacobs, 2010). Hence, various attempts have been made to improve the wear resistance of PE liners, such as enhancing the cross-linking of PE (CLPE) (Callaghan et al., 2008).

In the previous studies, we introduced a nanometer-scaled poly(2-methacryloyloxyethyl phosphorylcholine (MPC)) grafting layer on the surface of CLPE liners. We found that such type of grafting dramatically decreased the wear of the liner surface (Moro et al., 2009, 2006). In the present study, we investigated the effect of poly(MPC) grafting on the production of wear particles, using a hip wear simulator up to 15×10^6 cycles.

2. Materials and methods

2.1. Poly(MPC) grafting

Nanometer-scaled grafting (100–150 nm in thickness) of the poly (MPC) onto the PE liner surface was carried out by a photo-induced polymerization technique. The CLPE liners (K-MAX® CLQC; KYOCERA Medical Corp., Osaka, Japan) were immersed in an acetone solution containing 10 mg/mL of benzophenone for 30 s and then dried at room temperature to remove the acetone. Then, MPC (NOF Corp., Tokyo, Japan) (Ishihara et al., 1990) was dissolved in degassed pure water to obtain a 0.50 mol/L MPC aqueous solution, and the benzophenone-coated CLPE liners were immersed in this solution. Photoinduced graft polymerization was carried out on the CLPE liner surface using ultraviolet irradiation (UVL-400HA ultra-high-pressure mercury lamp; Riko-Kagaku Sangyo Co., Ltd., Funabashi, Japan) with an intensity of 5.0 mW/cm^2 at 60 °C for 90 min; subsequently, a filter (Model D-35; Toshiba Corp., Tokyo, Japan) was used to restrict the passage of ultraviolet light to wavelengths of 350±50 nm. After the poly (MPC)-grafted CLPE (MPC-CLPE) liners were polymerized, they were washed with pure water and ethanol and dried at room temperature. These specimens were then sterilized by 25-kGy gamma rays under N_2 gas (Kyomoto et al., 2008).

2.2. Hip joint simulator

A 12-station hip simulator (MTS Systems Corp., Eden Prairie, MN) with CLPE and MPC-CLPE liners, each with inner and outer diameters of 26 and 52 mm, respectively, was used for the hip simulator wear test performed according to the ISO Standard 14242-3. A Co–Cr alloy femoral head with a diameter of 26 mm (K-MAX® HH-02; KYOCERA Medical Corp.) was used as the femoral component. A biaxial rocking motion was applied to the head/cup interface via an offset bearing assembly with an inclined angle of +23°. Both the loading and motion were synchronized at 1 Hz. According to the double-peaked Paul-type physiologic hip load, the applied peak loads were 1793 and 2744 N (Paul, 1967). Bovine calf serum (25 vol%) diluted in distilled water was used as a lubricant. Sodium azide (10 mg/L) and EDTA (20 mM) were added to prevent microbial contamination and to minimize the formation of calcium phosphate on the implant surface.

The simulator was run up to 15×10^6 cycles. The liners were cleaned and weighed on a microbalance (Sartorius Genius ME215S, Sartorius AG, Goettingen, Germany) at intervals of 0.5×10^6 cycles. The lubricant was collected and stored at −20 °C for further analysis. Wear was determined from the weight loss of each liner and corrected by cyclically loaded soak controls according to the ISO Standard 14242-2. The wear rates were determined by linear regression.

After complete loading, morphological changes in the liner surface were measured using a three-dimensional (3D) coordinate measuring machine (BHN-305, Mitsutoyo Corp., Kawasaki, Japan) and reconstructed using 3D modeling software (Imageware, Siemens PLM Software Inc., TX, USA). The liner surface was analyzed using a confocal scanning laser microscope (OLS1200, Olympus, Tokyo, Japan), as previously reported.

The wear particles were isolated from the bovine serum solution. For isolating the wear particles from the lubricant, the lubricant was incubated with 5.0 mol/L of NaOH solution for 3 h at 65 °C after it was tested, in order to digest adhesive proteins that were degraded and precipitated. To avoid artifacts, contaminating proteins were removed by extraction with sugar solution (1.20 g/cm^3 and 1.05 g/cm^3) and isopropyl alcohol solutions (0.98 and 0.90 g/cm^3). After the lubricant was centrifuged at 25,500 rpm for 3 h at 5 °C, the particles were collected, subjected to sequential filtrations (minimum pore size of 0.1 μm) (Fisher et al., 2004; Tipper et al., 2006), and subsequently dried. The filter was then sputter coated with gold palladium and digitally imaged on a field emission scanning electron microscope (JSM-6330F, JEOL Datum Co., Ltd, Tokyo, Japan). An image-processing program (Scion image, Scion Corp., Frederick, MD) based on the

NIH image software was used to measure the total number, area, and volume of the wear particles per 10^6 cycles (Campbell et al., 1996; Dean et al., 1999). Two size descriptors, namely, the equivalent circle diameter (ECD) and the diameter (D), and two shape descriptors, namely, the aspect ratio (AR) and roundness (R), were used to define each wear particle, according to ASTM F1877-98. Each parameter is defined as follows. ECD is defined as the diameter of a circle with an area that is equivalent to that of one wear particle. Diameter is defined using the maximum dimensions determined by the SEM analysis. Aspect ratio is defined as the ratio of the major diameter to the minor diameter. It should be noted that the major diameter is the longest straight line that can be drawn between any two points on the outline. On the other hand, the minor diameter is the longest line that is perpendicular to the major diameter. Roundness is a measure of how closely a wear particle resembles a circle; its values range from 0 to 1, with a perfect circle having a roundness value of 1.

2.3. *Statistical analysis*

The significance of differences was determined by the student's *t*-test. All statistical analyses were performed using add-in software (Statcel 2; OMS publishing Inc, Tokorozawa, Japan) on a computerized worksheet (Microsoft Excel® 2003; Microsoft Corp, Redmond, WA).

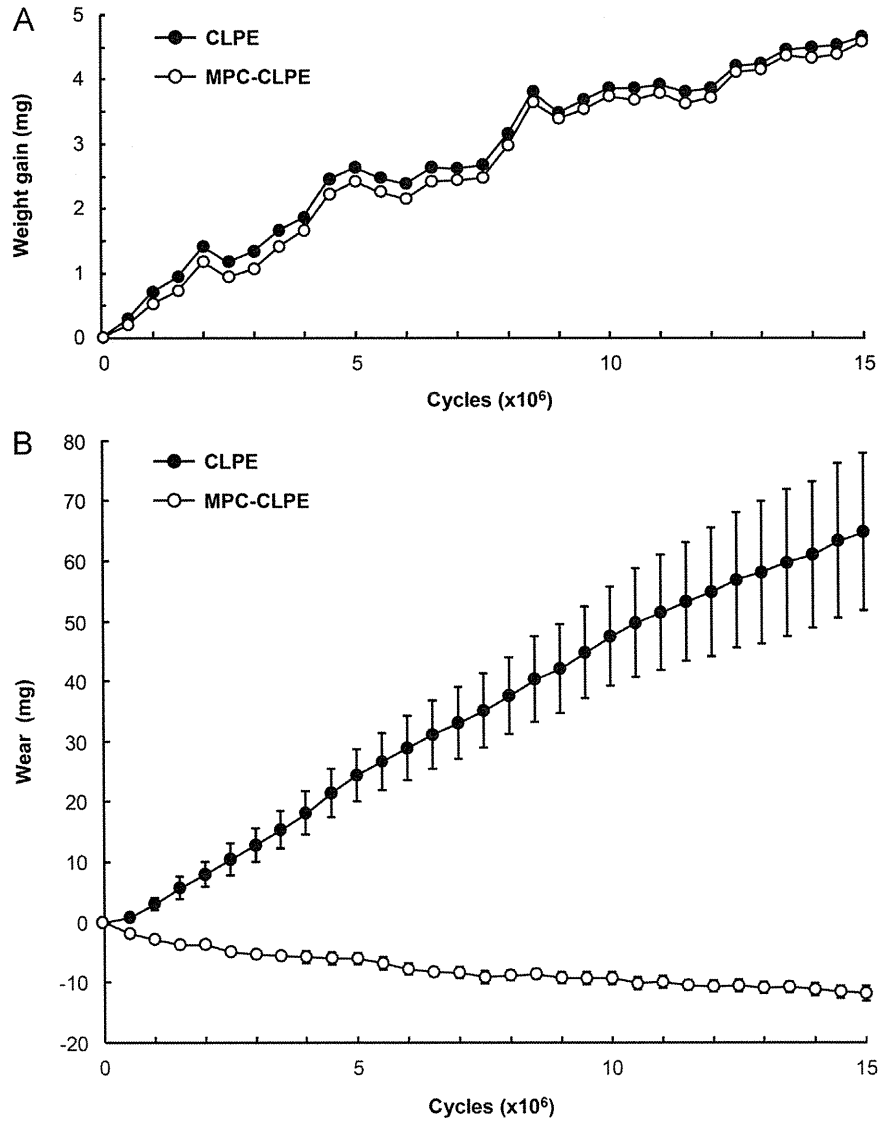

Fig. 1 – Wear amounts of cross-linked PE liners with or without MPC grafting in the THA simulator. (A) Load-soak controls. Fluid absorption of the liners that were axially loaded cyclically to the acetabular liners with the same pressure as the THA simulator, but without rotational motion. Data are expressed as means (symbols) for 2 inserts/group. (B) Time course of wear amount in the THA simulator during 15×10^6 cycles of rotational motion and axial loading against Co–Cr alloy femoral heads. The wear amount was estimated from the weight loss of the inserts after correction by the average weight gain in the respective load-soak controls (weight loss in the THA simulator+average of weight gain in the load-soak control). Data are expressed as means (symbols) ± standard deviation (SD) for 4 liners/group.

3. Results

Two types of load-soak control liners, which were only loaded axially to the femoral heads and without any rotational motion in the simulator, showed comparable weight gains during the 15×10^6 cycles, irrespective of whether poly(MPC) grafting (Fig. 1A) was carried out; this observation confirmed that weight gain was caused by the absorption of the fluid by the liner material, and not by the fluid that was retained in the surface poly(MPC) layer (Kyomoto et al., 2011; Moro et al., 2006, 2009). We then evaluated gravimetric wear by assessing the weight loss of the liners after correction by the average weight gain in the respective load-soak controls. The gravimetric analysis performed in the hip simulator study showed that the CLPE liners suffered from a total weight loss of 64.8 ± 11.7 mg (mean $\pm$ standard deviation) after 15×10^6 cycles of loading (Fig. 1B). In contrast, it was found that the MPC-CLPE liners continued to gain weight, showing a total weight gain of 13.1 ± 1.2 mg. This weight gain might be at least partially attributed to greater fluid (e.g., water, proteins, and lipids) absorption in the tested liners than in the load-soak controls, suggesting the underestimation of the load-soak control, as reported previously (Dumbleton et al., 2006; Muratoglu et al., 2001; Oral et al., 2006; Shen et al., 2011). When the wear rate was counted at an interval of every 10^6 cycles, poly(MPC) grafting was shown to maintain similar wear resistance in 0–1 ($p=0.0016$), 4–5 ($p=0.0019$), 9–10 ($p=0.0022$), 14–15 ($p=0.0075$), and the total ($p=0.002$) intervals (Table 1).

3D coordinate measurements of the MPC-CLPE liner surface revealed no or very little detectable volumetric wear, while the cross-linked PE liners suffered from substantial wears (Fig. 2A). The confocal scanning laser microscopic analysis of the liner surface showed that the original machine marks that are clearly visible before the loading still remained on the MPC-CLPE liner surface, although they were completely obliterated on the cross-linked PE liner.

Table 1 – Wear rate estimated by the corrected weight loss of CLPE and MPC-CLPE liners.

Test period (10^6 cycles)	Wear rate (mg/10^6 cycles)		p-value
	CLPE	MPC-CLPE	
0–1	2.34 ± 0.99	−3.43 ± 0.42	0.0016
4–5	5.47 ± 1.09	−1.05 ± 0.06	0.0019
9–10	4.85 ± 0.91	−0.47 ± 0.08	0.0022
14–15	3.60 ± 1.22	−0.73 ± 0.23	0.0075
Total	4.01 ± 0.87	−1.09 ± 0.08	0.0020

Data are expressed as mean ± standard deviation (SD).

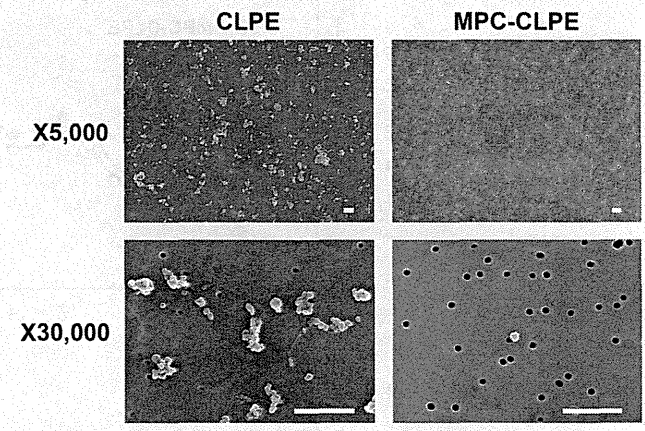

Fig. 3 – Scanning electron microscopic images of the wear particles from CLPE and MPC-CLPE liners. Low (top) and high (bottom) magnifications of the SEM images. Scale bars: 1.0 μm.

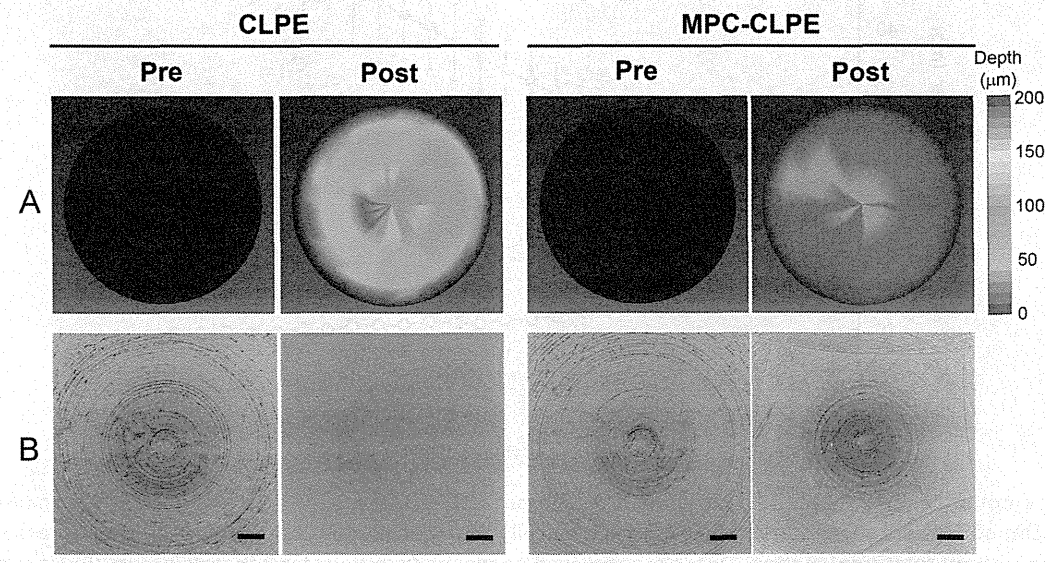

Fig. 2 – Optical findings of the surfaces of the two liners in the THA simulator. (A) Three-dimensional morphometric analyses of surfaces of the CLPE and MPC-CLPE liners before (pre) and after (post) 15×10^6 cycles. (B) Confocal scanning laser microscopic analysis of the contact areas in the two liner surfaces before (pre) and after (post) 15×10^6 cycles. Scale bars: 200 μm.

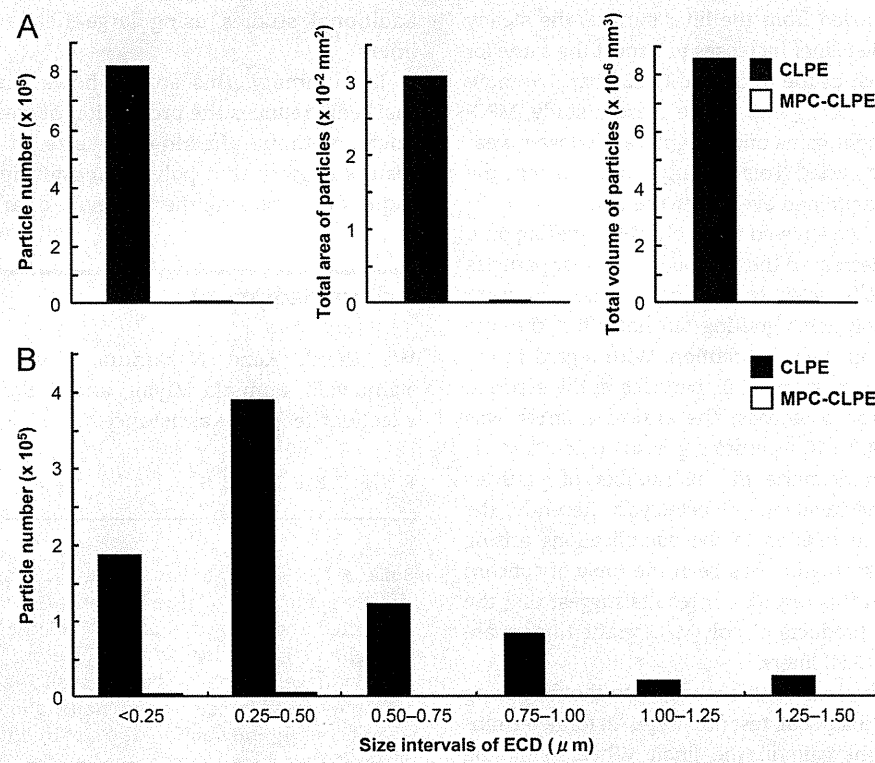

Fig. 4 – Analyses of wear particles isolated from lubricants in the hip simulator. (A) The graphs show the total number, area, and volume of the wear particles per 10^6 cycles. (B) Number of particles per 10^6 cycles in each size range of the equivalent circle diameter from CLPE and MPC-CLPE liners.

Table 2 – Assessments of the particle from CLPE and MPC-CLPE liners using size and shape descriptors.

Particle characterization	CLPE	MPC-CLPE	*p*-value
ECD (μm)	0.18±0.13	0.13±0.06	0.0000
Diameter (μm)	0.28±0.24	0.19±0.11	0.0001
Aspect ratio	2.31±0.79	2.10±0.51	0.0211
Roundness	0.83±0.22	0.92±0.13	0.0000

Two size descriptors, i.e., equivalent circle diameter (ECD) and diameter (D), and two shape descriptors, i.e., aspect ratio (AR) and roundness (R), were used to define each particle. Data are expressed as mean±standard deviation (SD).

The SEM analysis of the wear particles isolated from the lubricants indicated that poly(MPC) grafting dramatically decreased the total number, area, and volume of the wear particles by 99.3%, 99.9% and 99.9%, respectively (Fig. 3, Fig. 4A). However, there was no significant difference in the particle size distributions expressed by the equivalent circle diameter of each liner, and, in particular, from the SEM image, it was observed that particles with diameters less than 0.50 μm were present in the range of the highest frequency (Fig. 4C). In addition, there were no significant differences in the particle size descriptors, equivalent circle diameter ($p<0.0001$), and diameter ($p=0.0001$), as well as in the particle shape descriptors, aspect ratio ($p=0.0211$), and roundness ($p<0.0001$) (Table 2).

4. Discussion

An MPC molecule is one of the synthesized phospholipids and mimicks the surface of cellmembranes (Ishihara et al., 1990). Thus, poly(MPC) grafting onto medical devices makes their surface hydrophilic and biocompatible. Further, a thin film of water is formed under physiological conditions (Kitano et al., 2003). At the time of writing, the MPC polymers are applied to the surface of intravascular stents (Kuiper and Nordrehaug, 2000; Palmer et al., 2004), soft contact lenses (Selan et al., 2009), and artificial lungs and hearts (Kihara et al., 2003; Snyder et al., 2007) under the authorization of the U. S. Food and Drug Administration (FDA).

Because the PE liners are subjected to multidirectional heavy loads, we used a photoinduced radical graft polymerization technique for grafting. This technique produces a strong C–C covalent bond between a carbon atom of PE and the end-group of a poly(MPC) main chain. The advantages of this technique are that it not only results in the production of a uniform poly(MPC) layer (100–150 nm in thickness) but also causes a negligible effect on the physical and mechanical properties of the CLPE substrate (Ishihara et al., 2000; Kyomoto et al., 2007). Using this technique, we produced a new MPC-CLPE acetabular liner (Aquala® liner; KYOCERA Medical Corp.,) and the Japanese government (Ministry of Health, Labor, and Welfare) approved its clinical use in artificial hip joints in April 2011.

In addition to wear resistance, the durability of the nanometer-scaled poly(MPC) layer is also of major concern.

When this layer is removed from the liner surface, the steady wear rate of the MPC-CLPE liner increases to almost the same (or slight lower) level as that of the untreated CLPE liner (Kyomoto et al., 2011; Moro et al., 2006, 2010). In the present study, MPC-CLPE liners showed weight gains and a significantly lower wear rate during the 15×10^6 cycles. This finding confirmed that the poly(MPC) layer was maintained even after the test.

In the present study, we showed that poly(MPC) grafting onto the CLPE liner surface decreased the production of wear particles by 99% during 15×10^6 cycles of loading in the hip wear simulator. Moreover, poly(MPC) grafting did not affect the size of the wear particles and their distribution. With regard to the relationship between the number of PE particles in the synovial tissue and periprosthetic osteolysis, the critical number was reported to be around 1.0×10^{10} particles/g tissue (Kadoya et al., 1998). Thus, a marked decrease in the number of particles presumably reduces the incidence of osteolysis. Recently, the size of wear products in relation to the complications arising from metal-on-metal articulation has been the topic of concern (Hosman et al., 2010). In this regard, our results suggest that the influences of the wear products of poly(MPC)-grafted liners are similar to those of the CLPE liners.

There are three limitations of this study, with the first being underestimation in the load-soak test (ISO 14242-2) for determining the cause of weight gain in the liner. When using the gravimetric method, the weight loss in the tested liners is corrected for by subtracting the weight gain in the load-soak controls; however, this correction cannot be precisely achieved because only the tested liners are continuously subjected to load and motion. Fluid absorption in the tested liners is generally slightly higher than that in the load-soak controls. Consequently, the correction for fluid absorption through the use of the load-soak control as the correction factor leads to a slight underestimation of the actual weight loss. This underestimation has previously been reported, particularly in several reports on wear-resistant articulating surfaces (Dumbleton et al., 2006; Muratoglu et al., 2001; Oral et al., 2006; Shen et al., 2011). Because of this underestimation, wear could not be quantified by gravimetric analysis; however, weight change in the MPC-CLPE liners suggests the considerable wear-resistance of them. In the present study, we also analyzed the surface of the liner and the amount of wear particles generated from the liner, as well as confirmed that wear resistance of the acetabular liners was considerably improved by poly(MPC) grafting.

The second limitation of this study is the difference between the in vitro study and clinical settings. This difference was a matter of concern in the case of Hylamer (Graeter and Nevins, 1998; Huddleston et al., 2010). We do, however, believe that this issue is relatively insignificant as compared to that with regard to other materials, because poly(MPC)-grafted particles are biologically inert and do not cause the subsequent bone resorptive responses (Moro et al., 2004). Moreover, to the best of our knowledge, there are no reports on the complications of medical devices using MPC polymers.

The third limitation is that we used only Co–Cr alloy heads with a diameter of 26 mm. In clinical settings, there seems to be a tendency to choose large heads and thin acetabular liners in order to reduce the incidence of dislocation. We believe that this drawback is partially offset by the long duration of simulation. At present, we are conducting additional studies using large heads and thin acetabular liners.

In summary, this study shows that poly(MPC) grafting markedly reduces the production of wear particles from CLPE liners, without affecting the size of the particles. These results suggest that poly(MPC) grafting is a promising technique for increasing the longevity of artificial hip joints.

Acknowledgments

We thank Kozo Nakamura, Tomohiro Konno, Noboru Yamawaki, Fumiaki Miyaji, and Reiko Yamaguchi for their excellent technical assistance.

REFERENCES

Bozic, K.J., Kurtz, S.M., Lau, E., Ong, K., Vail, T.P., Berry, D.J., 2009. The epidemiology of revision total hip arthroplasty in the United States. Journal of Bone & Joint Surgery 91, 128–133.

Callaghan, J.J., Cuckler, J.M., Huddleston, J.I., Galante, J.O., 2008. How have alternative bearings (such as metal-on-metal, highly cross-linked polyethylene, and ceramic-on-ceramic) affected the prevention and treatment of osteolysis? Journal of the American Academy of Orthopaedic Surgeons 16 (Suppl. 1), S33–38.

Campbell, P., Doorn, P., Dorey, F., Amstutz, H.C., 1996. Wear and morphology of ultra-high molecular weight polyethylene wear particles from total hip replacements. Proceedings of the Institution of Mechanical Engineers Part H 210, 167–174.

Catelas, I., Jacobs, J.J., 2010. Biologic activity of wear particles. Instructional Course Lectures 59, 3–16.

Charnley, J., 1961. Arthroplasty of the hip. A new operation. Lancet 1, 1129–1132.

Dean, D.D., Schwartz, Z., Liu, Y., Blanchard, C.R., Agrawal, C.M., Mabrey, J.D., Sylvia, V.L., Lohmann, C.H., Boyan, B.D., 1999. The effect of ultra-high molecular weight polyethylene wear debris on MG63 osteosarcoma cells in vitro. Journal of Bone and Joint Surgery—American Volume 81, 452–461.

Dumbleton, J.H., D'Antonio, J.A., Manley, M.T., Capello, W.N., Wang, A., 2006. The basis for a second-generation highly cross-linked UHMWPE. Clinical Orthopaedics and Related Research 453, 265–271.

Fisher, J., McEwen, H.M., Tipper, J.L., Galvin, A.L., Ingram, J., Kamali, A., Stone, M.H., Ingham, E., 2004. Wear, debris, and biologic activity of cross-linked polyethylene in the knee: benefits and potential concerns. Clinical Orthopaedics and Related Research 428, 114–119.

Graeter, J.H., Nevins, R., 1998. Early osteolysis with Hylamer acetabular liners. Journal of Arthroplasty 13, 464–466.

Harris, W.H., 2004. Conquest of a worldwide human disease: particle-induced periprosthetic osteolysis. Clinical Orthopaedics and Related Research 429, 39–42.

Hosman, A.H., van der Mei, H.C., Bulstra, S.K., Busscher, H.J., Neut, D., 2010. Effects of metal-on-metal wear on the host immune system and infection in hip arthroplasty. Acta Orthopaedica 81, 526–534.

Huddleston, J.I., Harris, A.H., Atienza, C.A., Woolson, S.T., 2010. Hylamer vs conventional polyethylene in primary total hip arthroplasty: a long-term case-control study of wear rates and osteolysis. Journal of Arthroplasty 25, 203–207.

Ishihara, K., Iwasaki, Y., Ebihara, S., Shindo, Y., Nakabayashi, N., 2000. Photoinduced graft polymerization of 2-methacryloyloxyethyl phosphorylcholine on polyethylene membrane surface for obtaining blood cell adhesion resistance. Colloids and Surfaces B: Biointerfaces 18, 325–335.

Ishihara, K., Ueda, T., Nakabayashi, N., 1990. Preparation of phospholipid polymers and their properties as polymer hydrogel membrane. Polymer Journal 22, 355–360.

Jacobs, J.J., Roebuck, K.A., Archibeck, M., Hallab, N.J., Glant, T.T., 2001. Osteolysis: basic science. Clinical Orthopaedics and Related Research 393, 71–77.

Kadoya, Y., Kobayashi, A., Ohashi, H., 1998. Wear and osteolysis in total joint replacements. Acta Orthopaedica Scandinavica 278, 1–16.

Kihara, S., Yamazaki, K., Litwak, K., Litwak, P., Kameneva, M., Ushiyama, H., Tokuno, T., Borzelleca, D., Umezu, M., Tomioka, J., Tagusari, O., Akimoto, T., Koyanagi, H., Kurosawa, H., Kormos, R., Griffith, B., 2003. In vivo evaluation of a MPC polymer coated continuous flow left ventricular assist system. Artificial Organs 27, 188–192.

Kitano, H., Imai, M., Mori, T., Gemmei-Ide, M., Yokoyama, Y., Ishihara, K., 2003. Structure of water in the vicinity of phospholipid analogue copolymers as studied by vibrational spectroscopy. Langmuir 19, 10260–10266.

Kuiper, K.K., Nordrehaug, J.E., 2000. Early mobilization after protamine reversal of heparin following implantation of phosphorylcholine-coated stents in totally occluded coronary arteries. American Journal of Cardiology 85, 698–702.

Kyomoto, M., Moro, T., Konno, T., Takadama, H., Kawaguchi, H., Takatori, Y., Nakamura, K., Yamawaki, N., Ishihara, K., 2007. Effects of photo-induced graft polymerization of 2-methacryloyloxyethyl phosphorylcholine on physical properties of cross-linked polyethylene in artificial hip joints. Journal of Materials Science: Materials in Medicine 18, 1809–1815.

Kyomoto, M., Moro, T., Miyaji, F., Konno, T., Hashimoto, M., Kawaguchi, H., Takatori, Y., Nakamura, K., Ishihara, K., 2008. Enhanced wear resistance of orthopaedic bearing due to the cross-linking of poly(MPC) graft chains induced by gamma-ray irradiation. Journal of Biomedical Materials Research Part B: Applied Biomaterials 84, 320–327.

Kyomoto, M., Moro, T., Takatori, Y., Kawaguchi, H., Ishihara, K., 2011. Cartilage-mimicking, high-density brush structure improves wear resistance of crosslinked polyethylene: a pilot study. Clinical Orthopaedics and Related Research 469, 2327–2336.

Moro, T., Kawaguchi, H., Ishihara, K., Kyomoto, M., Karita, T., Ito, H., Nakamura, K., Takatori, Y., 2009. Wear resistance of artificial hip joints with poly(2-methacryloyloxyethyl phosphorylcholine) grafted polyethylene: comparisons with the effect of polyethylene cross-linking and ceramic femoral heads. Biomaterials 30, 2995–3001.

Moro, T., Takatori, Y., Ishihara, K., Konno, T., Takigawa, Y., Matsushita, T., Chung, U.I., Nakamura, K., Kawaguchi, H., 2004. Surface grafting of artificial joints with a biocompatible polymer for preventing periprosthetic osteolysis. Nature Materials 3, 829–836.

Moro, T., Takatori, Y., Ishihara, K., Nakamura, K., Kawaguchi, H., 2006. 2006 Frank Stinchfield Award: grafting of biocompatible polymer for longevity of artificial hip joints. Clinical Orthopaedics and Related Research 453, 58–63.

Moro, T., Takatori, Y., Kyomoto, M., Ishihara, K., Saiga, K., Nakamura, K., Kawaguchi, H., 2010. Surface grafting of biocompatible phospholipid polymer MPC provides wear resistance of tibial polyethylene insert in artificial knee joints. Osteoarthritis Cartilage 18, 1174–1182.

Muratoglu, O.K., Bragdon, C.R., O'Connor, D.O., Jasty, M., Harris, W.H., 2001. A novel method of cross-linking ultra-high-molecular-weight polyethylene to improve wear, reduce oxidation, and retain mechanical properties. Recipient of the 1999 HAP Paul Award. Journal of Arthroplasty 16, 149–160.

Oral, E., Christensen, S.D., Malhi, A.S., Wannomae, K.K., Muratoglu, O.K., 2006. Wear resistance and mechanical properties of highly cross-linked, ultrahigh-molecular weight polyethylene doped with vitamin E. Journal of Arthroplasty 21, 580–591.

Palmer, R.R., Lewis, A.L., Kirkwood, L.C., Rose, S.F., Lloyd, A.W., Vick, T.A., Stratford, P.W., 2004. Biological evaluation and drug delivery application of cationically modified phospholipid polymers. Biomaterials 25, 4785–4796.

Paul, J.P., 1967. Forces transmitted by joints in the human body. Proceedings of the Institution of Mechanical Engineers 181, 8–15.

Selan, L., Palma, S., Scoarughi, G.L., Papa, R., Veeh, R., Di Clemente, D., Artini, M., 2009. Phosphorylcholine impairs susceptibility to biofilm formation of hydrogel contact lenses. American Journal of Ophthalmology 147, 134–139.

Shen, F.W., Lu, Z., McKellop, H.A., 2011. Wear versus thickness and other features of 5-Mrad crosslinked UHMWPE acetabular liners. Clinical Orthopaedics and Related Research 469, 395–404.

Snyder, T.A., Tsukui, H., Kihara, S., Akimoto, T., Litwak, K.N., Kameneva, M.V., Yamazaki, K., Wagner, W.R., 2007. Preclinical biocompatibility assessment of the EVAHEART ventricular assist device: coating comparison and platelet activation. Journal of Biomedical Materials Research Part A 81, 85–92.

Tipper, J.L., Galvin, A.L., Williams, S., McEwen, H.M., Stone, M.H., Ingham, E., Fisher, J., 2006. Isolation and characterization of UHMWPE wear particles down to ten nanometers in size from in vitro hip and knee joint simulators. Journal of Biomedical Materials Research Part A 78, 473–480.

ORIGINAL ARTICLE

JBMR

Regulation of Bone Resorption and Sealing Zone Formation in Osteoclasts Occurs Through Protein Kinase B–Mediated Microtubule Stabilization

Takumi Matsumoto,[1] Yuichi Nagase,[1] Jun Hirose,[1] Naoto Tokuyama,[1] Tetsuro Yasui,[1] Yuho Kadono,[1] Kohjiro Ueki,[2] Takashi Kadowaki,[2] Kozo Nakamura,[1] and Sakae Tanaka[1]

[1]Department of Orthopaedic Surgery, Faculty of Medicine, The University of Tokyo, Tokyo, Japan
[2]Department of Diabetes and Metabolic Diseases, Faculty of Medicine, The University of Tokyo, Tokyo, Japan

ABSTRACT

We investigated the role of protein kinase B (Akt), a downstream effector of phosphatidylinositol 3-kinase, in bone-resorbing activity of mature osteoclasts. Treatment with a specific Akt inhibitor disrupted sealing zone formation and decreased the bone-resorbing activity of osteoclasts. The normal microtubule structures were lost and the Akt inhibitor reduced the amount of acetylated tubulin, which reflects stabilized microtubules, whereas forced Akt activation by adenovirus vectors resulted in the opposite effect. Forced Akt activation increased the binding of the microtubule-associated protein adenomatous polyposis coli (APC), the APC-binding protein end-binding protein 1 (EB1) and dynactin, a dynein activator complex, with microtubules. Depletion of *Akt1* and *Akt2* resulted in a disconnection of APC/EB1 and a decrease in bone-resorbing activity along with reduced sealing zone formation, both of which were recovered upon the addition of LiCl, a glycogen synthase kinase-3β (GSK-3β) inhibitor. The *Akt1* and *Akt2* double-knockout mice exhibited osteosclerosis due to reduced bone resorption. These findings indicate that Akt controls the bone-resorbing activity of osteoclasts by stabilizing microtubules via a regulation of the binding of microtubule associated proteins. © 2013 American Society for Bone and Mineral Research.

KEY WORDS: OSTEOCLAST; AKT; MICROTUBULE; OSTEOSCLEROSIS; KNOCKOUT MOUSE

Introduction

Cells which exhibit high motility, such as osteoclasts, dendritic cells, and macrophages, have actin-rich structures called podosomes, which mediate cell attachment and migration. Podosomes are composed of dense F-actin columns (the actin core) and a diffuse meshwork of F-actin surrounding the actin core (the actin cloud).[1] The osteoclast is a highly differentiated, multinucleated, bone-resorbing cell of hematopoietic origin. The podosomes in fully differentiated osteoclasts cultured on glass are observable at the cell periphery and form a ring like structure called the podosome belt.[2] The sealing zone is another ring-like F-actin–rich structure that bone-resorbing osteoclasts form on mineralized matrix.[3] The sealing zone serves as the part of the osteoclast that attaches to a target and provides an enclosed space known as a "resorption lacuna" between cells and bone. The membrane of the osteoclast circumscribed within this sealing zone is folded in order to form a ruffled border through which proton and matrix-degrading enzymes are released into the resorption lacunae. High-resolution electron microscopy revealed that the podosome belt and the sealing zone employ the same structural unit of F-actin and suggested that the difference between them is the result of the degree of compaction.[4] However, the regulatory mechanism underlying this compaction is still unknown.

Microtubules, one of the major components of the cytoskeleton, are polymers of α-tubulin and β-tubulin. Microtubules have a fast-growing end (plus-end) and slow-growing end (minus-end). In most cells, the minus-end binds to the microtubule organizing center and the plus-end extends toward the periphery. The plus-end microtubules switch from the assembly to the disassembly phase, and this phenomenon, *dynamic instability*, plays a crucial role in microtubule attachment to targets.[5] The plus-end possesses tracking proteins (+TIPs), a family of microtubule-associated proteins (MAPs) that accumulate and are involved in both the stabilization of the microtubule

Received in original form September 6, 2012; revised form November 9, 2012; accepted November 29, 2012. Accepted manuscript online December 13, 2012.
Address correspondence to: Sakae Tanaka, MD, PhD, Department of Orthopaedic Surgery, Faculty of Medicine, The University of Tokyo, Hongo7-3-1, Bunkyo-ku, Tokyo113-0033, Japan. E-mail: TANAKAS-ORT@h.u-tokyo.ac.jp

Journal of Bone and Mineral Research, Vol. 28, No. 5, May 2013, pp 1191–1202
DOI: 10.1002/jbmr.1844

and the interaction between the microtubule and the cell cortex. Mammalian osteoclasts have few centrosomal microtubule organizing centers, and the microtubules originate from pericentriolar matrix proteins on the nuclei.[6] In fully differentiated mammalian osteoclasts attached on glass, most of the nuclei are clustered at the cell periphery. From this location the microtubules radiate in a circular pattern.[6]

Recent studies have revealed that microtubules have an essential role in regulating the formation of podosome belts and sealing zones in osteoclasts.[7,8] In particular, the acetylated form of tubulin, which is an indication of stabilized tubulin, is considered to play an essential role in regulating osteoclast activity.[2,9] Hazama and colleagues[10] reported that the deacetylation of tubulin in osteoclasts is associated with the release of lytic granules required for bone-resorption. Destaing and colleagues[9] reported that the stabilization of the podosome belt and the sealing zone is associated with an increase in acetylated tubulin, which is in turn controlled by the Rho-mDia2-HDAC6 pathway, indicating the central role of HDAC6 in regulation of tubulin deacetylation. However, the specific mechanisms of the anchoring and stabilization of tubulin by MAPs in osteoclasts are not well understood.

Protein kinase B (Akt) is a major downstream effector of phosphatidylinositol 3-kinase (PI3K) and mediates cellular processes such as proliferation, migration, and survival. The Akt family members consist of Akt1/PKBα,Akt2/PKBβ, and Akt3/PKBγ. These isoforms are similar in structure and size, and are considered to be redundant to one another.[11] Akt1 and Akt2 are ubiquitously expressed in mammals, whereas Akt3 is expressed dominantly in the limited tissues such as the testis and brain.[11]

This study aimed to clarify the regulatory effect on the bone-resorbing activity of osteoclasts by the Akt pathway. Akt was found to positively regulate the bone-resorbing activity of osteoclasts by stabilizing microtubules and enhancing sealing zone formation. The microtubule stabilization effect of Akt was regulated by the binding of MAPs with microtubules through glycogen synthase kinase-3β (GSK-3β). Osteoclast-specific Akt1 and Akt2 double-deficient mice were shown to exhibit mild osteosclerosis caused by a decreased bone-resorbing function of osteoclasts. These results suggest that Akt plays an essential role in bone resorption by regulating the stable interaction between microtubules and the cell cortex, as well as regulating dynamic microtubule formation.

Subjects and Methods

Animals

Newborn and 5-week-old male C57BL/6J mice were purchased from Sankyo Labo Service Co. (Tokyo, Japan). The breeding and genotyping of the $Akt1^{fl/fl}$ and $Akt2^{fl/fl}$ mice (kindly provided by Morris J. Birnbaum, University of Pennsylvania) were performed as described.[12,13] To generate osteoclast-specific Akt1 and Akt2 double-conditional knockout (DKO) mice, we used cathepsin K-Cre mice (kindly provided by Shigeaki Kato, Soma Chuo Hospital), in which the Cre recombinase gene is knocked into the cathepsin K locus and specifically expressed in osteoclasts.[14] All animals were housed under specific pathogen-free conditions and treated with humane care under the approval of the Animal Care and Use Committee of the University of Tokyo.

Generation of osteoclasts and survival/bone resorption assay

Osteoclasts were generated using a coculture system, as described.[15] Briefly, when murine osteoblastic cells and bone marrow cells were cocultured on collagen gel–coated dishes in the presence of 10 nM 1α,25-dihydroxyvitamin D_3 [$1\alpha,25(OH)_2D_3$] and 1 μM prostaglandin E_2 (PGE_2), osteoclasts were differentiated on day 6 of culture. The cells were dispersed by treatment with 0.1% bacterial collagenase (Wako Pure Chemical, Tokyo, Japan) for 10 minutes and then used for the pit formation assay and the survival assay as follows. For the bone resorption assay, the cells were resuspended in α modified essential medium (α-MEM) containing 10% fetal bovine serum (FBS), replated on dentin slices, and cultured for 24 hours. After cells were removed by treating the dentin slices with 1 M NH_4OH, the resorption areas were visualized by staining with 1% toluidine blue. The resorption pit area was quantified using an image analyzing system.

The sealing zone formation on dentin slices was analyzed as follows. The cells were cultured on dentin slice as described in the previous paragraph. After 16 hours, the cells were fixed in PBS containing 4% paraformaldehyde for 10 minutes and then stained with tartrate-resistant acid phosphatase (TRAP). TRAP staining was performed at pH 5.0 in the presence of L(+)-tartaric acid using naphthol AS-MX phosphate (Sigma-Aldrich, St. Louis, MO, USA) in N-N dimethyl formamide as the substrate. Cells were then incubated for 30 minutes with rhodamine-conjugated phalloidin solution (Molecular Probes, Eugene, OR, USA) to visualize F-actin. Sealing zone formation on dentin slices was observed under fluorescence microscopy (Biozero; KEYENCE, Woodcliff Lake, NJ, USA). The sealing zone formation rate is represented as the proportion of the cells having an uninterrupted ring-like F-actin structure among the TRAP-positive multinucleated cells.

Triton cytoskeleton extraction

Extraction of the triton-insoluble cytoskeletal fraction was performed as described.[16] Briefly, osteoclast cultures were washed twice with ice-cold PBS, once with Buffer 1 (0.1 M PIPES [pH 6.9], 1 mM $MgSO_4$, 2 M glycerol, 2 mM EGTA, 0.02 trypsin inhibitory units per mL aprotinin) and then incubated for 3 minutes with Buffer 2 (Buffer1 + 0.2% [wt/vol] Triton X-100). This fraction is referred to as the Triton X-100–solubule or "cytosolic" fraction. The Triton X-100–insoluble remainders were washed twice with Buffer 3 (1 M piperazine-N,N′-bis(2-ethanesulfonic acid) [PIPES] [pH 6.9], 1 mM $MgSO_4$, 2 M glycerol, 0.02 trypsin inhibitory units per mL aprotinin), and dissolved with Ca^{2+}-containing medium (0.1 M PIPES [pH 6.9], 1 mM $MgSO_4$, 5 mM $CaCl_2$, 0.02 trypsin inhibitory units per mL aprotinin). The lysate was centrifuged at 12,000 *g* for 10 minutes at 4°C, and the supernatant was collected. This fraction is referred to as the Triton-X-100–insoluble fraction or "Triton cytoskeleton" fraction. The lysates were used for immunoblotting analysis.

Western blotting and immunoprecipitation

All the extraction procedures were performed at 4°C or on ice. Cells were washed with ice-cold PBS, and proteins were extracted with TNE buffer (1% NP-40, 10 mM Tris-HCl [pH 7.8], 150 mM NaCl, 1 mM EDTA, 2 mM $Na3VO_4$, 10 mM NaF, and 10 μg/mL of aprotinin). The lysates were clarified by centrifugation at 12,000*g* for 10 minutes. For Western blotting analysis, lysates were subjected to SDS-PAGE with 7.5% to 15% Tris-Glycin gradient gels or 15% Tris-Glycin gels, and transferred onto nitrocellulose membranes (Bio-Rad, Hercules, CA, USA). After blocking with 6% milk/TBS-T, membranes were incubated with primary antibodies to phospho-Akt (Ser473), Akt, phospho-GSK-3β (Ser9), GSK-3β, β-Catenin, Akt1, Akt2 (Cell Signaling Technology Inc., Beverly, MA, USA), APC, CLIP-170, Lis1 (Santa Cruz Biotechnology Inc., Santa Cruz, CA, USA), p150 Glued (BD Biosciences Inc., San Diego, CA, USA), EB1, acetylated tubulin, α-tubulin, β-actin (Sigma-Aldrich, St. Louis, MO, USA), or CLASP2 (ProteinTech Group, Chicago, IL, USA), followed by horseradish peroxidase (HRP)-conjugated goat anti-mouse immunoglobulin G (IgG), goat anti-rabbit IgG (Promega, Madison, WI, USA), and donkey anti-goat IgG (Santa Cruz Biotechnology). Immunoreactive bands were visualized with ECL Plus (Amersham, Pittsburgh, PA, USA), according to the manufacturer's instructions. The blots were stripped by incubation for 20 minutes in stripping buffer (2% SDS, 100 mM 2-mercaptoethanol, and 62.5 mM Tris-HCl [pH 6.7]) at 50°C, and then reprobed with additional antibodies.

Immunoprecipitation was performed by incubating 500 mg of total cell protein lysate with 2 μg of antibody for 2 hours on ice and then adding 20 μL of protein G-agarose. After incubation for 1 hour at 4°C with end-over-end mixing, the immune complex was recovered by centrifugation and washed five times with buffer containing 20 mM HEPES-NaOH, pH 7.4, 150 mM NaCl, 10 mM EDTA, and 0.02% NP-40. The immunoprecipitates were then subjected to SDS-PAGE and Western blot analysis.

Expression constructs and gene transduction

The adenovirus vectors used in the experiments and the genes carried by the vectors were as follows: AxTb-YFP (tubulin-yellow fluorescence fusion protein gene), AxEB1-YFP (the EB1-yellow fluorescence fusion protein gene), AxCre (Cre recombinase gene), and $AxAkt^{CA}$ (the constitutively active Akt1 gene). AxTb-YFP and AxEB1-YFP were provided by Dr. Takao Nakata (Tokyo Medical and Dental University, Tokyo, Japan). $AxAkt^{CA}$ was provided by Dr. Hideki Katagiri (Tohoku University, Miyagi, Japan). Constitutively active Akt1 was generated by adding a myristoylation signal sequence to its N terminus. The control virus (Ax1W1) was provided by Dr. Izumu Saito (The University of Tokyo, Tokyo, Japan). Viral titers were determined by the end point dilution assay, and the viruses were used at 50 multiplicity of infection (MOI). The infection of adenovirus vectors into osteoclasts was carried out following the method described.[17] In short, on day 4 of the culture, when osteoclasts began to appear, mouse cocultures were incubated for 1 hour at 37°C with a small amount of α-MEM containing the recombinant adenoviruses at the desired MOI. Cells were then washed twice with PBS and further incubated at 37°C in α-MEM containing 10% FBS, 10 nM $1\alpha,25(OH)_2D_3$, and 1 μM PGE_2. Experiments were performed 36 hours after the infection.

Nocodazole treatment

Osteoclasts infected with AxTb-YFP were purified by treating them with 1 μM nocodazole for 30 minutes. After 30 minutes, the cells were washed three times with PBS, and then fixed with 4% paraformaldehyde to detect nocodazole-resistant tubulin. Cells were fixed with 4% paraformaldehyde for 0, 30, 60, 90, and 120 minutes after the washout of nocodazole for observation of the microtubule reorganization.

Immunofluorescence and time-lapse imaging

For live imaging experiments, osteoclasts cultured on glass coverslips were infected with AxTb-YFP and incubated with α-MEM containing 5 μg/mL Hoechst 33258 for 30 minutes. Osteoclasts were treated with nocodazole as described in Nocodazole treatment above, and incubated with α-MEM, or with α-MEM containing 1 μM Akt inhibitor IV (Calbiochem, San Diego, CA, USA), or with α-MEM containing 20 mM LiCl. Osteoclasts were placed in a thermostat containing chamber for microscopic analysis, allowing the temperature to be maintained at 37°C throughout the experiment, and cells were imaged under fluorescence microscopy (BZ-8100; KEYENCE). Images were collected at 90-second intervals for 120 minutes.

Radiographic, micro–computed tomography, and histomorphometric analyses

Plain radiographs were taken using a soft X-ray apparatus (CMB-2; SOFTEX, Tokyo, Japan). Micro–computed tomography (μCT) scanning of the distal femur was performed using a ScanXmate-L090 Scanner (Comscantechno Co., Ltd., Yokohama, Japan). Three-dimensional microstructural image data were reconstructed and structural indices were calculated using TRI/3D-BON software (RATOC Systems, Osaka, Japan).

Tissues were fixed in 4% paraformaldehyde/PBS, decalcified in 10% EDTA, embedded in paraffin, and cut into 3-μm-thick sections. Hematoxylin and eosin (H&E) staining was performed according to the standard procedure. Osteoclasts were identified by TRAP staining. Histomorphometric analysis was performed in undecalcified sections from 0.2 mm below the growth plate to a point 1.125 mm distal of the primary spongiosa of the proximal tibia. For double-labeling, mice were injected subcutaneously with 16 mg/kg body weight of calcein on 4 days and 1 day before euthanasia.

Statistical analysis

Each series of experiments was repeated at least three times. The results are expressed as the mean ± SD. Statistical analyses were performed using a two-tailed unpaired Student's *t* test or ANOVA analysis.

Results

An Akt inhibitor impairs the bone-resorbing activity and cytoskeletal organization of osteoclasts

We first examined the effect on osteoclasts of the Akt inhibitor IV, which was designed to target an adenosine triphosphate (ATP)-binding site of a kinase immediately upstream of Akt but downstream of PI3K. Treatment with 1 μM of the Akt inhibitor significantly reduced the pit formation without affecting the survival of osteoclasts (Fig. 1*A*, *B*). The proportion of osteoclasts containing sealing zones was significantly decreased by Akt inhibitor treatment (Fig. 1*C*, *D*). These results suggest that Akt regulates the bone-resorbing activity of osteoclasts by its effect on sealing zone formation.

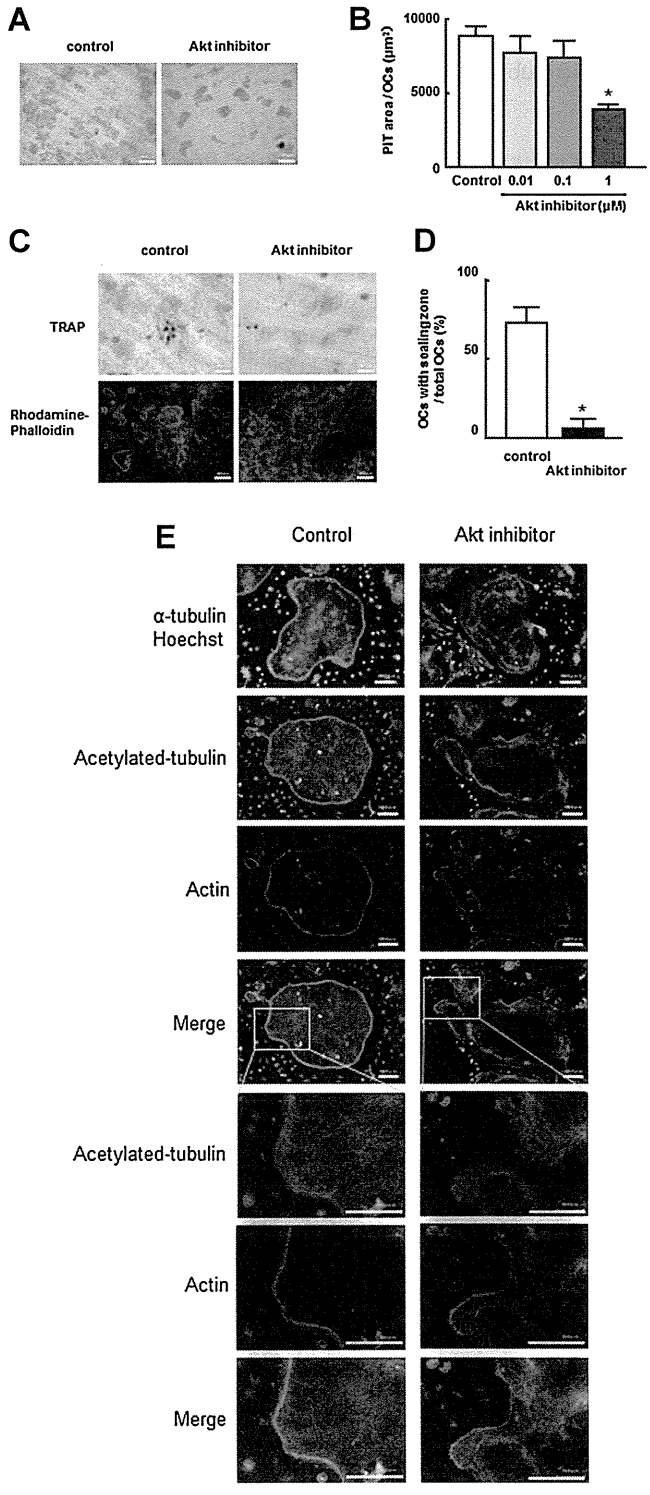

Recent studies have demonstrated that the formation of both podosome belts and sealing zones in osteoclasts is associated with an increase in tubulin acetylation corresponding to microtubule stabilization.[9] We therefore compared the structures of the podosome belts and acetylated tubulin between osteoclasts with and without the Akt inhibitor under fluorescent microscopy. The microtubules in mature osteoclasts on glass consist of two forms; one is a circular pattern of microtubules at the cell periphery, and the other is a pattern of microtubules radiating from the central cytoplasm to the cell periphery.[18] Acetylated tubulin was distributed uniformly along these structures in mature osteoclasts, and the Akt inhibitor disrupted these orderly microtubule structures (Fig. 1*E*). The podosome belt positioning at the cell periphery in the untreated osteoclasts was rearranged in the cytoplasm after Akt inhibitor treatment (Fig. 1*E*). These results suggest that Akt critically regulates the structure and stability of microtubules in osteoclasts.

The forced activation of Akt results in the stabilization of microtubules and increased bone-resorbing activity

We then evaluated the effect of a gain-of-function of Akt by introducing the constitutively active Akt1 gene into osteoclasts using an adenovirus vector (AxAkt^{CA}). The forced activation of Akt by adenovirus infection increased the phosphorylation level of GSK-3β, a downstream effector of Akt, and also the amount of acetylated tubulin (Fig. 2*A*). The proportion of osteoclasts containing sealing zones were increased by Akt^{CA} expression, and their bone-resorbing activity was significantly enhanced (Fig. 2*B*, *C*). Immunofluorescence staining showed that a thick layer of acetylated tubulin was observed in the cell periphery of osteoclasts infected with AxAkt^{CA} (Fig. 2*D*). Nocodazole treatment disrupted microtubule organization in control

Fig. 1. Effect of the Akt inhibitor IV on bone-resorbing activity and cytoskeletal organization of osteoclasts. (*A*) Osteoclasts generated on collagen gel-coated dishes were replated on dentine slices and cultured for an additional 24 hours with the indicated dose of the Akt inhibitor IV. The resorption areas were visualized by staining the dentine slices with 1% toluidine blue, and measured using an image analysis system. Scale bars = 100 μm. (*B*) Resorption pit area per osteoclast. $^*p < 0.01$ versus untreated control. (*C*) Osteoclasts were cultured on dentin slices for 16 hours with or without 1 μM of Akt inhibitor IV and then subjected to TRAP and rhodamine-conjugated phalloidin staining. Scale bars = 50 μm. (*D*) Proportion of osteoclasts obtained as in *C* with a sealing zone. $^*p < 0.01$ versus control. (*E*) Osteoclasts generated on glass coverslip were cultured for 5 hours with or without 1 μM of Akt inhibitor IV and then visualized under fluorescence microscopy after staining for acetylated tubulin (green) and actin (red), except for the top panel, in which α-tubulin (was) is stained in green and nuclei were stained blue with Hoechst 33258. The last three panels are enlarged views of the boxed areas. Scale bars = 100 μm.